

# Integrated GC-MS/MS Metabolomics in Cardiovascular Disease: Targeted Nitro-Oleic Acid Quantification Meets Untargeted Profiling

Yasmin Elshoura, Magy Herz,\* Mohamed Z. Gad, and Rasha Hanafi



Cite This: <https://doi.org/10.1021/acs.analchem.5c05647>



Read Online

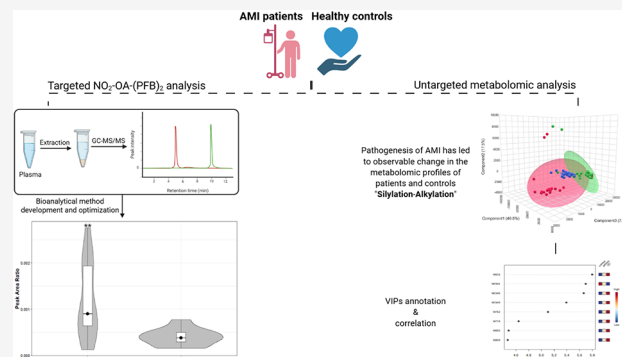
ACCESS |

Metrics & More

Article Recommendations

Supporting Information

**ABSTRACT:** In recent decades, interest in nitrated fatty acids ( $\text{NO}_2\text{-FAs}$ ) has grown due to their role as endogenous signaling molecules involved in health and disease. As a result, their metabolic profiling has gained increasing attention. For metabolite analysis, GC-MS/MS offers greater sensitivity and robustness than LC-MS/MS, with more reliable annotation libraries. This study investigates metabolic dysregulation in cardiovascular disease (CVD) patients by using advanced metabolomics. A novel GC-MS/MS method for profiling  $\text{NO}_2\text{-FAs}$  was developed, showing improved precision using 17-BrHDA as an internal standard compared to previous HDA-based methods. It is also the first report of alkylation and silylation derivatization of 17-BrHDA, demonstrating superior GC-MS sensitivity for pentafluorobenzyl-alkylated fatty acids over their silylated counterparts in positive ion mode. Untargeted metabolomics was applied to plasma samples from acute myocardial infarction (AMI) patients and healthy controls using both derivatization techniques. Multivariate analysis (PCA and PLS-DA) revealed distinct metabolic profiles. Key metabolites, identified based on VIP scores, were annotated via the Human Metabolome Database and literature. Findings highlight the complementary nature of both derivatization approaches for comprehensive plasma metabolome analysis. Notably,  $\text{NO}_2\text{-OA}$  levels were significantly elevated ( $p < 0.01$ ) in AMI patients, indicating its possibility to be utilized as a cardiovascular biomarker. This study represents the first use of alkylation derivatization in untargeted metabolomics for AMI and introduces a highly sensitive GC-MS/MS method with an innovative internal standard and optimized derivatization for cardiovascular biomarker discovery. The method demonstrates the potential to discriminate between groups of patients and healthy subjects.



## INTRODUCTION

Omics is a branch of biological sciences focused on the comprehensive analysis of genes, mRNAs, proteins, and metabolites—known respectively as genomics, transcriptomics, proteomics, and metabolomics.<sup>1</sup> Among these, metabolomics most closely reflects the phenotype<sup>2–4</sup> as metabolite variations often mirror changes in the genome, transcriptome, or proteome. Currently, metabolomics is extensively applied in biological systems due to its strong potential in biomarker discovery.<sup>1</sup>

Mass spectrometry (MS) coupled with chromatographic techniques is central to metabolomics. Among them, gas chromatography–mass spectrometry (GC-MS) is pivotal because it separates compounds based on volatility and vapor pressure, offering reproducible fragmentation patterns and access to more robust spectral libraries compared to liquid chromatography–mass spectrometry (LC-MS). Additionally, chemical derivatization prior to GC analysis enhances the metabolite volatility and thermal stability, enabling the detection of a broader range of metabolites. As such, GC-MS provides a compelling combination of sensitivity (greater than NMR) and reliability (greater than LC-MS).<sup>5</sup>

In recent years, nitrated fatty acids ( $\text{NO}_2\text{-FAs}$ ) have garnered increasing attention as endogenous signaling molecules with regulatory roles in health and disease.<sup>6</sup> Their biological activity largely involves reversible post-translational modifications of cysteine residues in proteins via Michael addition reactions (nitroalkylation),<sup>7</sup> modulating protein function, signaling pathways, and cellular responses.

Endogenously,  $\text{NO}_2\text{-FAs}$  act as electrophilic Michael acceptors, modifying thiol groups on transcriptional regulators, thereby influencing gene expression and metabolic or inflammatory signaling.<sup>8</sup> They originate from various fatty acid backbones, and multiple positional isomers have been identified both in vitro and in biological samples.<sup>6,9,10</sup> The most studied forms include nitro-oleic acid ( $\text{NO}_2\text{-OA}$ ), nitro-

Received: September 11, 2025

Revised: January 13, 2026

Accepted: January 14, 2026

linoleic acid ( $\text{NO}_2\text{-LA}$ ), and nitro-conjugated linoleic acid ( $\text{NO}_2\text{-cLA}$ ).<sup>11–13</sup>

However, reported endogenous  $\text{NO}_2\text{-FA}$  levels vary due to differences in analytical techniques and sample preparation.<sup>14</sup> Some studies report micromolar levels,<sup>11,12</sup> while others find picomolar to low nanomolar concentrations, which aligns with findings by Tsikas et al., using a validated GC-MS/MS method for  $\text{NO}_2\text{-OA}$  isomers.<sup>14,15</sup> This method, employing solid-phase extraction (SPE) and HPLC pretreatment, identified 9- $\text{NO}_2\text{-OA}$  and 10- $\text{NO}_2\text{-OA}$  in healthy plasma at  $0.88 \pm 0.29$  nM and  $0.94 \pm 0.26$  nM, respectively.<sup>15</sup> When liquid–liquid extraction (LLE) was used without pretreatment, sensitivity slightly declined, with concentrations of  $0.306 \pm 0.044$  and  $0.316 \pm 0.033$  nM, respectively, still consistent with earlier data.<sup>16</sup> Using a validated LC-MS/MS method, Herz et al. later measured  $\text{NO}_2\text{-OA}$  and  $\text{NO}_2\text{-LA}$  at higher values— $12.6 \pm 6$  nM and  $3.2 \pm 1.7$  nM, respectively.<sup>16,17</sup>

To meet the demand for more accurate biomarkers in cardiovascular disease (CVD), this study develops and optimizes a novel GC-MS/MS method for quantifying  $\text{NO}_2\text{-OA}$  in plasma from acute myocardial infarction (AMI) patients compared with healthy controls. For the first time, we introduce 17-brominated heptadecanoic acid (17-BrHDA) as an internal standard in  $\text{NO}_2\text{-FA}$  analysis, improving sensitivity, reproducibility, and cost-efficiency over conventional heptadecanoic acid (HDA). We also propose a novel derivatization technique using pentafluorobenzyl bromide (PFB-Br) to overcome the low sensitivity of the  $\text{NO}_2\text{-FA}$  methyl esters. Finally, we apply both silylation and alkylation to enhance metabolite annotation and biomarker identification.

## MATERIALS AND METHODS

### Materials

Alkane standard mixture for performance tests of GC systems C10–C40 (all even), glacial acetic acid, heptadecanoic acid (HDA), 2,3,4,5,6-Pentafluorobenzyl bromide (PFB-Br), and pyridine were obtained from Sigma-Aldrich (Schnelldorf, Germany). HPLC-grade methanol (MeOH), HPLC-grade acetonitrile (ACN), HPLC-grade diethyl ether (DEE), and N-Methyl-N-(trimethylsilyl)trifluoroacetamide (MSTFA) with 1% trimethylchlorosilane (TMCS) were from Merck (Darmstadt, Germany). Cis-9-nitro-9-octadecenoic acid (9- $\text{NO}_2\text{-OA}$ ) was purchased from Cayman Chemical (Ann Arbor, MI, USA) and stored at  $-20^\circ\text{C}$ . Butylated hydroxytoluene (BHT) and N,N-diisopropylethylamine (DIPEA) were from Lobachemie (Mumbai, India). 17-Bromoheptadecanoic acid (17-BrHDA) was obtained from BLD Pharmatech GmbH (Shanghai, China). HPLC-grade toluene was purchased from Fischer (Germany).

### Bioanalytical Method Development

**Sample Size Calculation.** Patients' and controls' data were assumed to be non-normally distributed based on a retrospective study calculation. Therefore, the Mann–Whitney U test was utilized to calculate sample size by G-power. In the untargeted study, the effect size was 0.8, the data distribution was two-tailed with an alpha of 0.05, a power of 0.8, and a 1:1 allocation ratio. The predicted sample size was 54 participants divided into 2 groups.

In the targeted study, the retrospective approach was utilized to calculate the effect size, where the previously reported levels of nitro fatty acids were input as mean and standard deviation, followed by the calculation of an estimated effect size. The

input data were  $21.7 \pm 9.8$  nM for AMI patients and  $12.6 \pm 6$  nM for healthy controls.<sup>17</sup> This estimated effect size of 1.12 and other parameters such as tails and allocation ratio were kept similar to those of the untargeted study. The predicted sample size for the targeted study was 30 participants divided into 2 equal groups.

**Blood Samples Collection.** Blood samples were collected from 27 AMI patients recruited from the National Heart Institute in Giza, Egypt and 27 healthy controls (Table 1). All

**Table 1. Characteristics of Study Participants**

	AMI patients STEMI (n = 17) NSTEMI (n = 10)	Healthy controls (n = 27)
Age (years; Median $\pm$ IQR)	53 $\pm$ 14	46 $\pm$ 6
Sex (male/female)	19/8	19/8
Smokers	14	4
Hypertensive	11	0
Diabetic	9	0

participants provided informed consent, which was approved by the Ethics Committee at the German University in Cairo (Project ID:PCH-2022-02-MM). Plasma was isolated by centrifugation at 3000 g for 10 min at  $4^\circ\text{C}$  and stored at  $-80^\circ\text{C}$  until sample preparation and analysis. All participants, including both patients and controls, were under ad libitum feeding conditions and were not adhering to any controlled dietary regimens or consuming ketogenic meals. Individuals were excluded from the study if they had any acute or chronic severe illnesses (e.g., renal failure or hepatic impairment) or were receiving medications known to affect lipid metabolism.

**Plasma Samples Preparation.** For the targeted study (Table 2), plasma samples were thawed on ice, and 250  $\mu\text{L}$

**Table 2. Summary of the Sample Treatment Protocol in Untargeted and Targeted Analysis**

	Untargeted	Targeted
Plasma	200 $\mu\text{L}$	250 $\mu\text{L}$
IS	20 $\mu\text{L}$ (5 $\mu\text{g/mL}$ )	7.5 $\mu\text{L}$ (5 $\mu\text{g/mL}$ )
First vortexing	30 s	30 s
20% acidified MeOH	200 $\mu\text{L}$	250 $\mu\text{L}$
Vortex	1 min	1 min
Incubation ( $4^\circ\text{C}$ )	20 min	20 min
0.02% BHT in DEE	2400 $\mu\text{L}$	1666 $\mu\text{L}$
Second vortexing	3 min	3 min
Centrifuge ( $4^\circ\text{C}$ , 4000 rpm)	15 min	15 min
Filter	1000 $\mu\text{L}$ (for each derivatization reaction)	1500 $\mu\text{L}$
Concentrate to dryness under vacuum at room temperature		

aliquots were spiked with 7.5  $\mu\text{L}$  of 5  $\mu\text{g/mL}$  of the internal standard 17-BrHDA (IS) and vortexed for 30 s. For deproteination, methanol (MeOH) acidified with 20% (v/v) acetic acid was added and vortexed for 1 min followed by incubation at  $4^\circ\text{C}$  for 20 min. Afterward, 1666  $\mu\text{L}$  of diethyl ether (DEE) containing the antioxidant 0.02% BHT were added and vortexed for 3 min followed by centrifugation at 4000 g for 15 min at  $4^\circ\text{C}$ . A volume of 1500  $\mu\text{L}$  of the upper layer was transferred and filtered into Eppendorf tubes, concentrated under vacuum at room temperature until complete dryness and stored at  $-20^\circ\text{C}$  until analysis.

Derivatization by PFB-Br was carried out on the day of analysis, where 100  $\mu\text{L}$  acetonitrile (ACN), 20  $\mu\text{L}$  DIPEA, and 20  $\mu\text{L}$  PFB-Br in ACN (30% v/v) were added on the residue, vortexed for 30 s, and incubated in the heat block for 1 h at 30  $^{\circ}\text{C}$  increased to 35  $^{\circ}\text{C}$  for an additional 30 min. The samples were vacuum concentrated to dryness at room temperature then reconstituted in 15  $\mu\text{L}$  toluene. The samples were transferred into insert-containing glass vials for GC-MS/MS analysis.

For the untargeted study (Table 2), plasma samples were prepared similar to the targeted study. A volume of 1000  $\mu\text{L}$  of the upper layer was filtered and split into two Eppendorf tubes, where one is intended for silylation and the other for the alkylation derivatization reaction. The liquid was concentrated under a vacuum until complete dryness and stored at -20  $^{\circ}\text{C}$  until analysis. Derivatization reactions were carried out on the day of analysis (Table 3). A quality control (QC) sample was

**Table 3. Summary of the Protocol for Derivatization Reactions**

Reaction type	Untargeted		Targeted
	Silylation	Alkylation	Alkylation
Solvents and reagents	40 $\mu\text{L}$ MSTFA + 1% TMCS	100 $\mu\text{L}$ ACN 20 $\mu\text{L}$ DIPEA 20 $\mu\text{L}$ PFB-Br in ACN (30% v/v)	100 $\mu\text{L}$ ACN 20 $\mu\text{L}$ DIPEA 20 $\mu\text{L}$ PFB-Br IN ACN (30% v/v)
vortex	30 s	30 s	30 s
Heat block (1 h, 600 rpm)	80 $^{\circ}\text{C}$	30 $^{\circ}\text{C}$	30 $^{\circ}\text{C}$ (then extra 30 min at 35 $^{\circ}\text{C}$ )
Vacuum concentrator	—	30 min	30 min
Solvents added	10 $\mu\text{L}$ Pyridine	50 $\mu\text{L}$ Toluene	15 $\mu\text{L}$ Toluene
Final volume	50 $\mu\text{L}$	50 $\mu\text{L}$	15 $\mu\text{L}$

obtained by pooling 100  $\mu\text{L}$  from each of the 27 AMI patients and 27 healthy controls to make a total of 5400  $\mu\text{L}$  that were divided and treated similarly.

**Silylation Derivatization.** Samples were treated with 40  $\mu\text{L}$  of MSTFA + 1% TMCS, vortexed for 30 s, and incubated in the heat block for 1 h at 80  $^{\circ}\text{C}$ . Afterward, 10  $\mu\text{L}$  of pyridine was added followed by centrifugation at 1000 g for 5 min at 20  $^{\circ}\text{C}$ . The samples were transferred into insert-containing glass vials for GC-MS/MS analysis.

**Alkylation Derivatization.** Samples were treated with 100  $\mu\text{L}$  of ACN, 20  $\mu\text{L}$  of DIPEA, and 20  $\mu\text{L}$  of PFB-Br in ACN (30% v/v), vortexed for 30 s, and incubated in the heat block for 1 h at 30  $^{\circ}\text{C}$ . The samples were concentrated under vacuum for 30 min then reconstituted in 50  $\mu\text{L}$  of toluene, vortexed for 3 min, and centrifuged at 20  $^{\circ}\text{C}$  for 5 min at 1000 g. The samples were transferred into insert-containing glass vials for GC-MS/MS analysis.

#### Gas Chromatography Tandem Mass Spectrometry

Analysis in EI mode was performed by a triple quadrupole mass spectrometer ThermoQuest TQ 7010B directly interfaced with a Trace 8890 series gas chromatograph equipped with an autosampler AS 7693A. Separation took place in a 30-m long fused-silica capillary column DB-5MS (250  $\mu\text{m}$   $\times$  0.25  $\mu\text{m}$  film thickness) using helium as the carrier gas at a constant flow rate of 1 mL/min. In the targeted analysis, the oven temperature ramped from 150 to 300  $^{\circ}\text{C}$  at a rate of 6  $^{\circ}\text{C}/\text{min}$  and was held at the maximum temperature for 1 min to make a total run time of 26 min. The ion source and mass transfer line

were kept at 230 and 300  $^{\circ}\text{C}$ , respectively. Electron energy was set to 70 eV with MRM transitions 689 > 327 for NO<sub>2</sub>-OA-(PFB)<sub>2</sub> derivative and 349 > 81 for 17-BrHDA-PFB derivative. The dwell time and collision energy were 50 ms and 15 eV for each ion in GC-MS/MS. Sample aliquots (1  $\mu\text{L}$ ) were injected in splitless mode. In the untargeted approach, similar parameters were utilized with full scan mode in a mass range of 50–900 Da. The oven temperature ramped from 70 to 300  $^{\circ}\text{C}$  at 6  $^{\circ}\text{C}/\text{min}$  and was held at the maximum temperature for 1 min resulting in a total run time of 39 min.

#### Liquid Chromatography Tandem Mass Spectrometry

To further confirm the identity of the NO<sub>2</sub>-OA-(PFB)<sub>2</sub> derivative, UPLC-ESI-MS analysis was performed using a Waters ACQUITY Xevo TQD system, consisting of an ACQUITY UPLC H-Class system and a Xevo TQD triple-quadrupole mass spectrometer with an electrospray ionization (ESI) interface (Waters Corp., Milford, MA, USA). An Acquity BEH C18 column (100  $\times$  2.1 mm, 1.7  $\mu\text{m}$ ) was used to separate analytes (Waters, Ireland) by a mobile phase composed of 0.1% formic acid in H<sub>2</sub>O (A) and 0.1% formic acid in ACN (B) flowing at 200  $\mu\text{L}/\text{min}$  in gradient mode. The starting composition was 5% B for 1 min linearly ramped to 100% over 10 min and sustained for 2 min, then returned to the start composition in 3 min and conditioning for 1 min. The MS scan was carried out at a capillary voltage of 3.5 kV, cone voltage of 20 V, radio frequency (RF) lens voltage of 2.5 V, source temperature of 150  $^{\circ}\text{C}$ , and desolvation gas temperature of 500  $^{\circ}\text{C}$ . Nitrogen was used as the desolvation and cone gas at a flow rate of 1000 and 20 L/h, respectively. System operation and data acquisition were controlled using Mass Lynx 4.1 software (Waters).

#### Data Acquisition and Integration

For the untargeted analysis, pooled QC samples were used to assess the repeatability of the analytical batch and to remove metabolic features suffering from high drift in signal, retention time, or accurate mass prior to data processing.<sup>18</sup> Extracted plasma samples were injected in a predetermined order, starting by a solvent run to check for background signals and contamination. A blank run was used to filter the data from artifact signals attributed to the derivatizing reagents. Four QC samples were injected at the start of the analytical order to condition the analytical platform before important samples were analyzed. The 54 subject samples were randomly injected, bracketed by QC samples every 3 injections.

#### Data Processing

Data processing was performed using the open-source MS-Dial software ver. 4.9 (<http://prime.psc.riken.jp/compms/msdial/main.html>) and the MetaboAnalyst online platform (<https://www.metaboanalyst.ca/>). Data processing produces a matrix of features with associated retention times, accurate masses, and chromatographic peak areas.

The raw data underwent an extensive processing approach to facilitate comprehensive statistical analysis and biological interpretation. The metabolomics workflow, predominantly executed with MS-Dial, included the following essential steps:

**Data Conversion and Initial Parameterization.** Raw data files obtained from MassHunter Qualitative Analysis (v.10.0) were converted into the open source.abf data format with the Reifys Analysis Base File Converter. Subsequently, within MS-Dial, samples were categorized into their appropriate classes (patient, control, quality control, and blank),

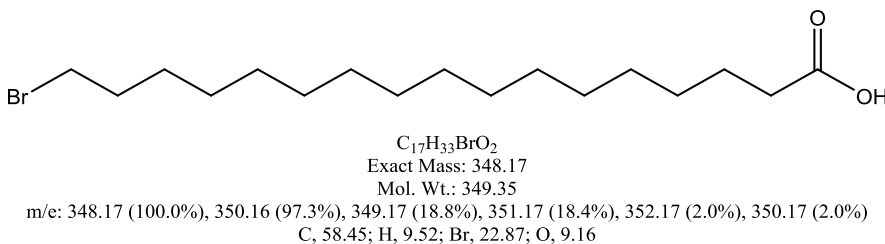


Figure 1. 17-Bromohedadecanoic acid chemical structure.

which were essential for subsequent processing and analysis. The data collection parameters were established with a mass range of 50–900 Da and a retention time range of 6–39.3 min, employing multithreading for enhanced efficiency.

**Feature Detection and Alignment.** Metabolite characteristics were identified using a minimum peak height of 1000 amplitude. Detected chromatograms were further deconvoluted into discrete peaks, utilizing a sigma window value of 0.5 and an EI spectra threshold of 1 amplitude. To ensure a thorough comparison of samples, the corresponding peaks were aligned using the QC sample as the reference file, with a retention time tolerance of 0.1 min (peculiar to the DB-5MS column) and  $m/z$  tolerance of 0.5. 17-BrHDA was spiked into all samples as an internal standard at a uniform concentration to reduce variability in sample processing and analytical platform performance.

**Data Curation and Normalization.** Subsequent to alignment, a gap-filling procedure was executed to replace absent peaks caused by detection inadequacies or alignment inaccuracies, employing the specified  $m/z$  and retention time limits. Subsequently, blank-run features were eliminated by a filtering technique to eradicate the analytical noise.

Data normalization took place in MS-Dial using LOESS (locally estimated scatterplot smoothing). This nonparametric regression method was utilized to fit a smooth curve to data points, hence diminishing sensitivity to outliers and adjusting for systematic analytical variances among samples. This stage attempted to enhance data distribution and comparability, which are essential conditions for parametric statistical analysis.

**Data Transformation and Scaling for Statistical Analysis.** The processed data were exported as a.csv file for additional multivariate statistical analysis using MetaboAnalyst. Features with low repeatability in QC samples (RSDs greater than 30%) were excluded. A square root transformation was employed to mitigate heteroscedasticity and improve the symmetry of the skewed distributions. Subsequent to transformation, mean centering was executed, wherein variables were adjusted by their mean. This scaling method seeks to correct discrepancies in fold changes across various metabolites by converting data into concentration fluctuations relative to the scaling factor, thus, facilitating accurate statistical comparisons.

### Statistical Analysis

In the targeted study, peak area ratios were tested for normality using the Shapiro Wilk test and for significance using the Student's *t*-test implemented in RStudio v.2024.12.0. In the untargeted analysis, multivariate data analysis, namely principal component analysis (PCA) and partial least-squares discriminant analysis (PLS-DA), was performed using MetaboAnalyst from where variables influencing projections (VIPs) were determined.

### Data Annotation Using Human Metabolome Database (HMDB)

VIPs annotation was performed on the human metabolome database (HMDB) based on reliable matching of GC-MS spectra, type of column (semi-standard nonpolar), derivatization technique, and finally retention index, which normalizes instrument variables. In addition to this, the false discovery rate (FDR) adjustment was applied using the Benjamini–Hochberg method.

The linear temperature-programmed retention index (LTPRI) established by Van der Dool and Kratz was calculated with eq 1, where  $I^T$  is the retention index and  $z$  is the number of carbons in the peak eluting before the analyte of interest (determined by injecting an alkane standard using the same instrument parameters of the untargeted study),  $T_i$  is the temperature at which the analyte of interest elutes,  $T_z$  is the temperature at which the peak of the alkane standard before the analyte of interest elutes, and  $T_{z+1}$  is the temperature at which the peak of the alkane standard after the analyte of interest elutes. The retention temperatures were replaced by their corresponding retention times.<sup>19</sup>

$$I^T = 100z + 100 \frac{T_i - T_z}{T_{z+1} - T_z} \quad (1)$$

### Correlation of VIPs in AMI Patients

The annotated VIPs that effectively distinguished between patients and controls were assessed for correlation in AMI patients using the Spearman correlation test in RStudio v.2024.12.0, with significance determined for those exhibiting strong correlations.

## RESULTS AND DISCUSSION

### Targeted NO<sub>2</sub>–OA Study

**17-Bromohedadecanoic Acid as a Novel Internal Standard in NO<sub>2</sub>–FAs Analysis.** Using an internal standard is necessary to compensate for variability in sample processing and analytical platform operation. Heptadecanoic acid (HDA) was previously used as a low-cost internal standard with structural similar to NO<sub>2</sub>–FAs.<sup>17,20</sup> Although HDA is not produced endogenously in humans,<sup>21,22</sup> yet its use as an internal standard has been criticized<sup>23</sup> because it is present in ingested dairy products and hence can be found in plasma from food. On the other hand, the stable isotope-labeled analogues of NO<sub>2</sub>–FAs are used as internal standards,<sup>16</sup> yet their cost is challenging in low-budget projects. A research gap emerges in the need to find a low-cost internal standard structurally resemblant to long-chain fatty acids, neither biosynthesized endogenously nor consumed in the diet, and possessing a better fragmentation pattern than HDA in both LC-MS/MS and GC-MS/MS. In our study, 17-BrHDA

(Figure 1) met these criteria along with a specific fragmentation pattern due to the presence of a bromide group, which provides characteristic product ions with  $m/z$  79 and 81. Although 17-BrHDA is a 17C chain fatty acid similar to HDA, the bromide functionality enhances structural similarity to  $\text{NO}_2$ -FAs composed of an 18C chain fatty acid with a nitro group. The resemblance between the bromide and nitro as functional groups is explained by the *Craig plot*, which relates substituent factors such as hydrophobicity and electronic characteristics to reveal biosisosteric substituents for studies of quantitative structure–activity relationship (QSAR).<sup>24</sup> This supports our hypothesis that 17-BrHDA and  $\text{NO}_2$ -OA would have close retention affinities, where bromide and nitro groups are in the same quadrant of the *Craig plot*, reflecting similarity in substituent factors.

Table 4 compares HDA,<sup>16,17,20</sup> 17-BrHDA (a brominated analog), and stable isotope-labeled nitro fatty acids ( $^{13}\text{C}/^{15}\text{N}$ -labeled  $\text{NO}_2$ -FAs) as internal standards (IS) for the quantification of endogenous nitro fatty acids using GC-MS/MS.<sup>15,25–28</sup>

Although stable isotope-labeled  $\text{NO}_2$ -FAs (e.g.,  $^{13}\text{C}/^{15}\text{N}$ - $\text{NO}_2$ -OA) serve as the definitive internal standards for accurate quantitative analysis owing to their isotopic equivalence and enhanced correction of matrix and ionization effects, their prohibitive cost and restricted commercial availability may hinder routine use. On the contrary, 17-BrHDA presents a viable and analytically sound alternative, characterized by significant chemical stability, unique mass spectrum characteristics, and availability from commercial suppliers. Its structural and physical similarity to endogenous nitrated fatty acids along with dependable chromatographic efficacy establishes 17-BrHDA as an economical and adaptable substitute for both targeted and untargeted metabolomic studies. These findings collectively endorse the use of 17-BrHDA as an appropriate internal standard in investigations lacking isotope-labeled equivalents or in which these alternatives are economically unfeasible.

**Solubility Study of the Novel Internal Standard.** The solubility of 17-BrHDA ( $\log P = 6.8$ ) was evaluated to determine the ideal solvent for the preparation of stock solutions. The compound exhibited insolubility in MeOH ( $\log P = -0.5$ ) at ambient temperature, despite sonication for 30 min at 30 °C. In 2-propanol ( $\log P = 0.3$ ), it exhibited limited solubility and salting out at –20 °C. Ultimately, DEE ( $\log P = 0.9$ ) exhibited superior solvent characteristics for 17-BrHDA, dissolving up to 1 mg/mL readily. Furthermore, no salting out occurred during storage at –20 °C.

To validate these solubility results, solutions of 17-BrHDA were prepared in each solvent (MeOH, IPA, and DEE) at a nominal concentration of 50 µg/mL or at the maximum attainable concentration as 50 µg/mL was not feasible due to solubility constraints. The solutions were subsequently tested by chromatography to determine the precise quantity of the dissolved compound. The chromatographic signal-to-noise ratios derived from these tests provide a quantitative assessment of the effective concentration and, consequently, the solubility. The S/N values were 4 for MeOH, 3.5 for IPA, and 44.5 for DEE, indicating that DEE is the most effective solvent due to its enhanced capacity to dissolve 17-BrHDA, yielding a significantly stronger and clearer chromatographic signal. It is worth mentioning that 17-BrHDA had nearly identical retention times across the three different solvents in which it was injected, with an RSD of approximately 0.1%.

**Table 4. Comparison between HDA, 17-BrHDA, and Stable Isotope-Labeled Nitro Fatty Acids as Internal Standards**

Parameter	HDA	17-BrHDA	$\text{NO}_2$ -FA
Structural similarity to $\text{NO}_2$ -FA	Low; absence of nitro group; saturated fatty acid analogue	Moderate; comparable chain length; bromine provides a mass label but exhibits distinct chemical properties compared to the nitro group.	High; isotopologue identical except for isotopic label
Analytical accuracy and correction ability	Moderate to low; adjusts only for extraction, without derivatization or matrix effects particular to $\text{NO}_2$ -FAs.	Moderate; robust EI signature, yet insufficient correction of nitro-specific deficits	Excellent; rectifies extraction, derivatization, and matrix effects (benchmark standard)
Endogenous Presence	Yes (oxidized DHA metabolite)	No (synthetic)	No (synthetic isotope)
Stability in matrix	Moderate (oxidation-prone)	High	High
Cost and availability	Relatively low; widely accessible from commercial vendors	Moderate; available from chemical suppliers (Sigma, Ambeed)	Elevated; restricted commercial availability or customized synthesis necessary.
Chemical and storage stability	Stable (saturated)	Stable; brominated chain exhibits resistance to oxidation	Similar to analyte (requires storage <–20 °C inert atmosphere)
Efficiency in derivatization and EI fragmentation	High for general FA analysis; nonspecific for the $\text{NO}_2$ group	High; distinctive Br isotope pattern aids detection	Optimal; compatible derivatization and fragmentation pattern, yet weak EI signals.
Behavior in biological matrices	Suitable for comprehensive fatty acid extraction; inadequate matrix correction for nitro species.	Intermediate; lipophilicity comparable to analytes.	Optimal; coextracts and coelutes with endogenous nitro fatty acids.
Novelty	Generic FA IS; is extensively utilized in traditional GC methodologies.	Emerging alternative IS (unique isotope pattern)	Cutting-edge, endorsed for validated quantitative assays
Overall suitability	Low; Requires control of endogenous levels	Good practical compromise	Best analytical performance

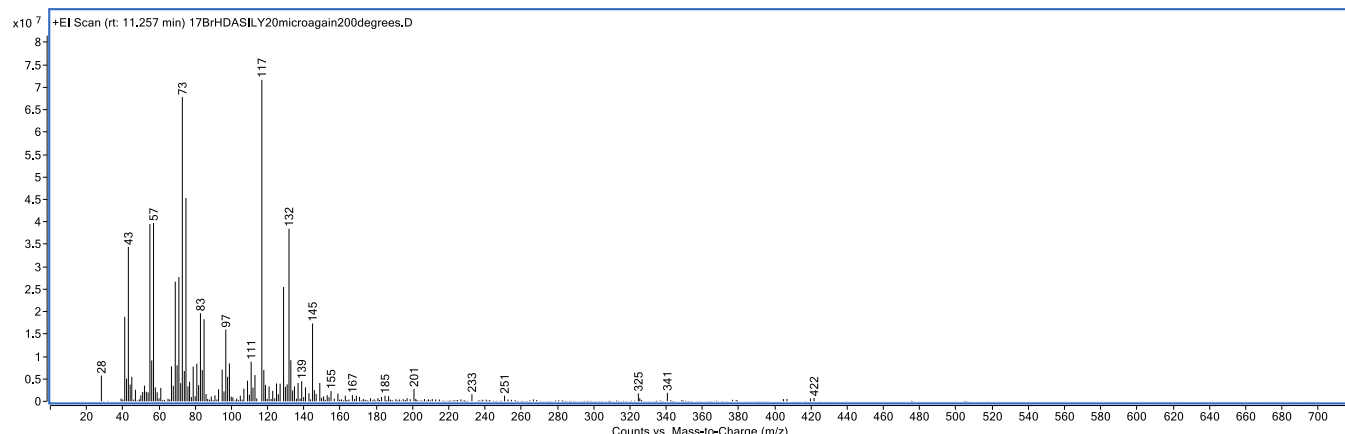


**Figure 2.** Experimental mass spectrum of the 17-BrHDA TMS derivative with parent ions  $\sim 420$  and  $422\text{ }m/z$  and product ions  $325$  and  $341\text{ }m/z$ .

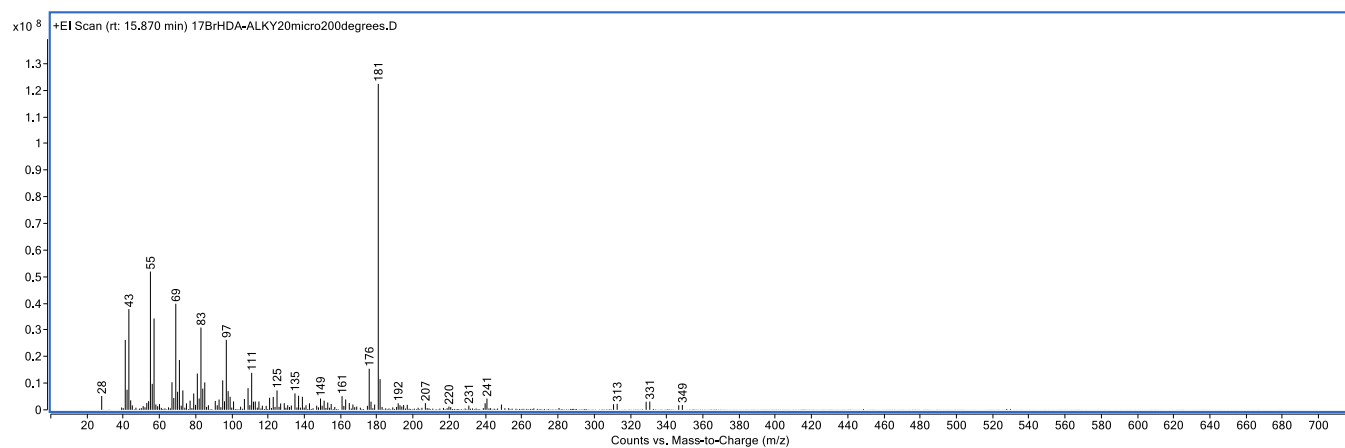


**Figure 3.** Experimental EI mass spectrum of the 17-BrHDA PFB derivative with parent ions  $m/z$   $528$  and  $m/z$   $530$  and product ions  $m/z$   $349$  and  $m/z$   $331$ .

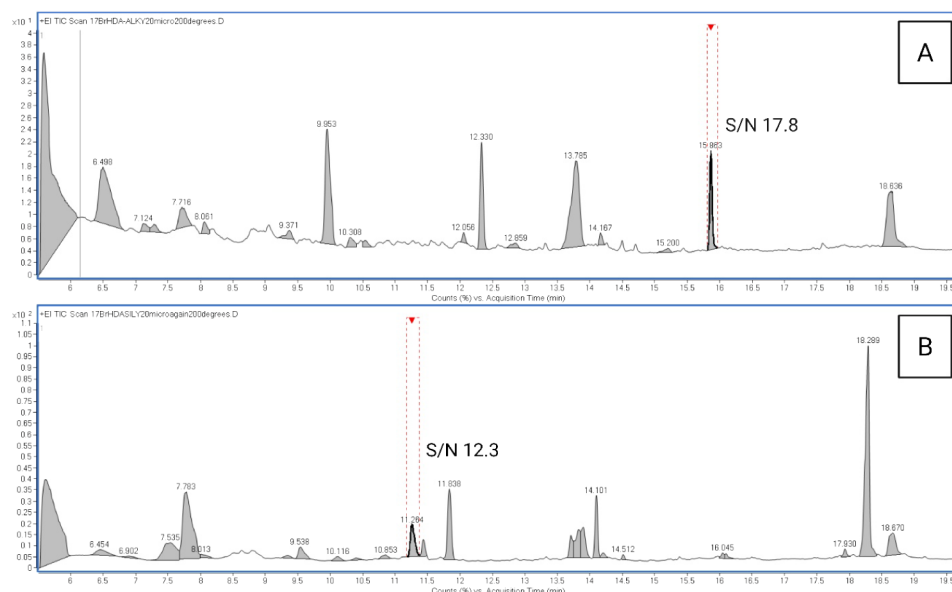


**Figure 4.** GC-MS analysis of the 17-BrHDA PFB derivative with S/N of 17.8 (A), and the 17-BrHDA TMS derivative with S/N of 12.3 (B) in full scan mode.

**Identification of 17-Bromoheptadecanoic Acid by GC-MS/MS.** Silylation and alkylation were attempted to derivatize 17-BrHDA to examine their relative sensitivity. The predicted

fragments of silylated and alkylated 17-BrHDA were confirmed in the mass spectra showing the 2 isotopic peaks of bromine (Br-79: Br-81, 1:1) (Figures 2 and 3).

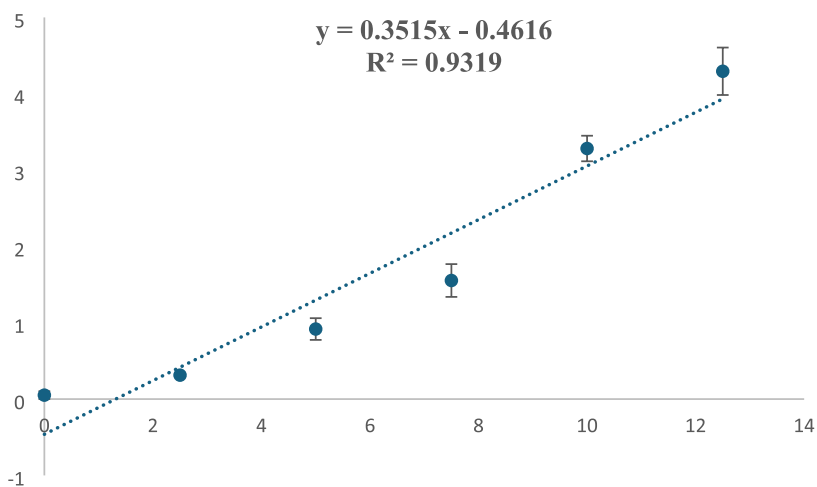


Figure 5. 17-BrHDA linearity results.

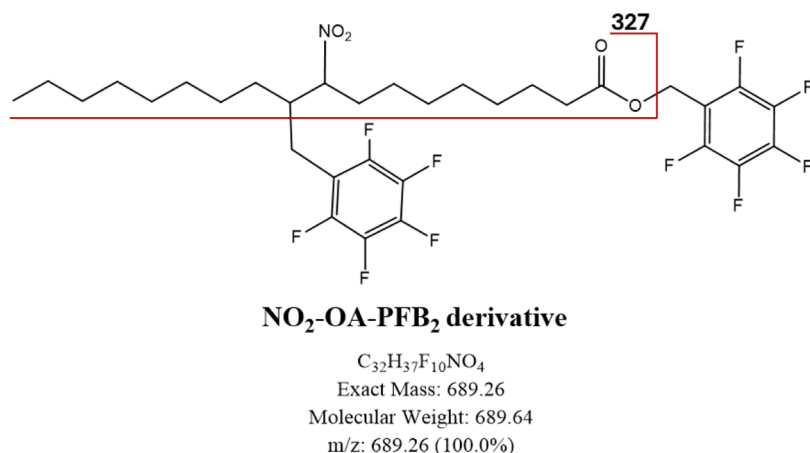


Figure 6. Hypothesized product of the dual-site derivatization of NO<sub>2</sub>-OA using PFB-Br (precursor ion *m/z* 689, product ion *m/z* 327).

It was found that the 17-BrHDA PFB derivative gave an S/N of 17.8, while the 17-BrHDA TMS derivative gave an S/N of 12.3 (Figure 4) implying that alkylation using PFB-Br as a derivatizing reagent gives better sensitivity to long-chain fatty acids than silylation when determined by EI GC-MS/MS. As a result, the alkylation derivatization reaction using PFB-Br was chosen for the targeted approach to ensure the detectability of the low endogenous levels of nitro fatty acids.

Further confirmation of the 17-BrHDA PFB peak (Figure 4A) was done by testing linearity using HDA as an internal standard in MRM mode. The monitored transitions were 349 > 81 for 17-BrHDA and 269 > 181 for HDA in the range (2.5  $\mu$ g/mL–12.5  $\mu$ g/mL) (Figure 5). Five calibration samples were prepared in triplicates and spiked with HDA. A linear response was observed for 17-BrHDA with an *R*<sup>2</sup> value of 0.9319 and *p* < 0.01 over the studied range.

The brominated internal standard demonstrated significant chemical stability, exhibiting no observable degradation or transformation following several freeze–thaw cycles. It was kept in its solid form at ambient temperature,<sup>29</sup> whereas stock solutions formulated in diethyl ether were preserved at –20 °C to avoid solvent evaporation and alterations in concentration. The compound exhibited stability under the applied derivatization and extraction conditions, maintaining constant retention time and peak area throughout replicate injections

(%RSD < 15% at 10–12.5  $\mu$ g/mL and up to 30% at lower concentrations).

#### GC-MS/MS Analysis of NO<sub>2</sub>-OA

**Dual-Site Derivatization of NO<sub>2</sub>-OA with PFB-Br during Alkylation.** Our EI-GC-MS/MS analysis successfully identified a novel dibenzylated derivative of NO<sub>2</sub>-OA with a precursor ion at *m/z* 689 (Figure 6). This derivative was formed through a hypothesized dual-site attack by PFB groups on both the alkene and carboxylic acid functional groups. By monitoring the product ion at *m/z* 327, linear calibration was obtained, resulting in an *R*<sup>2</sup> value of 0.9408 (Figure 9). The two benzyl moieties from the precursor ion are likely to have been lost, resulting in the formation of this fragment ion.

In contrast, the formation of a mono-PFB derivative of NO<sub>2</sub>-OA was reported in previous attempts employing ECNICI GC-MS/MS.<sup>15</sup> In addition, our endeavors to replicate the EI GC-MS/MS detection of this mono-PFB derivative by monitoring the MRM transitions *m/z* 326 > 197, 195, 168, 46 and 507 > 326, 297, 305<sup>9,15</sup> were unsuccessful. This discrepancy implies that the reaction between NO<sub>2</sub>-OA and PFB-Br under our experimental conditions favors dual-site derivatization, potentially due to differences in instrumental parameters. The formation of the *m/z* 689 derivative observed in our study, which was not reported in prior EI GC-MS/MS investigations, is a plausible explanation supported by the

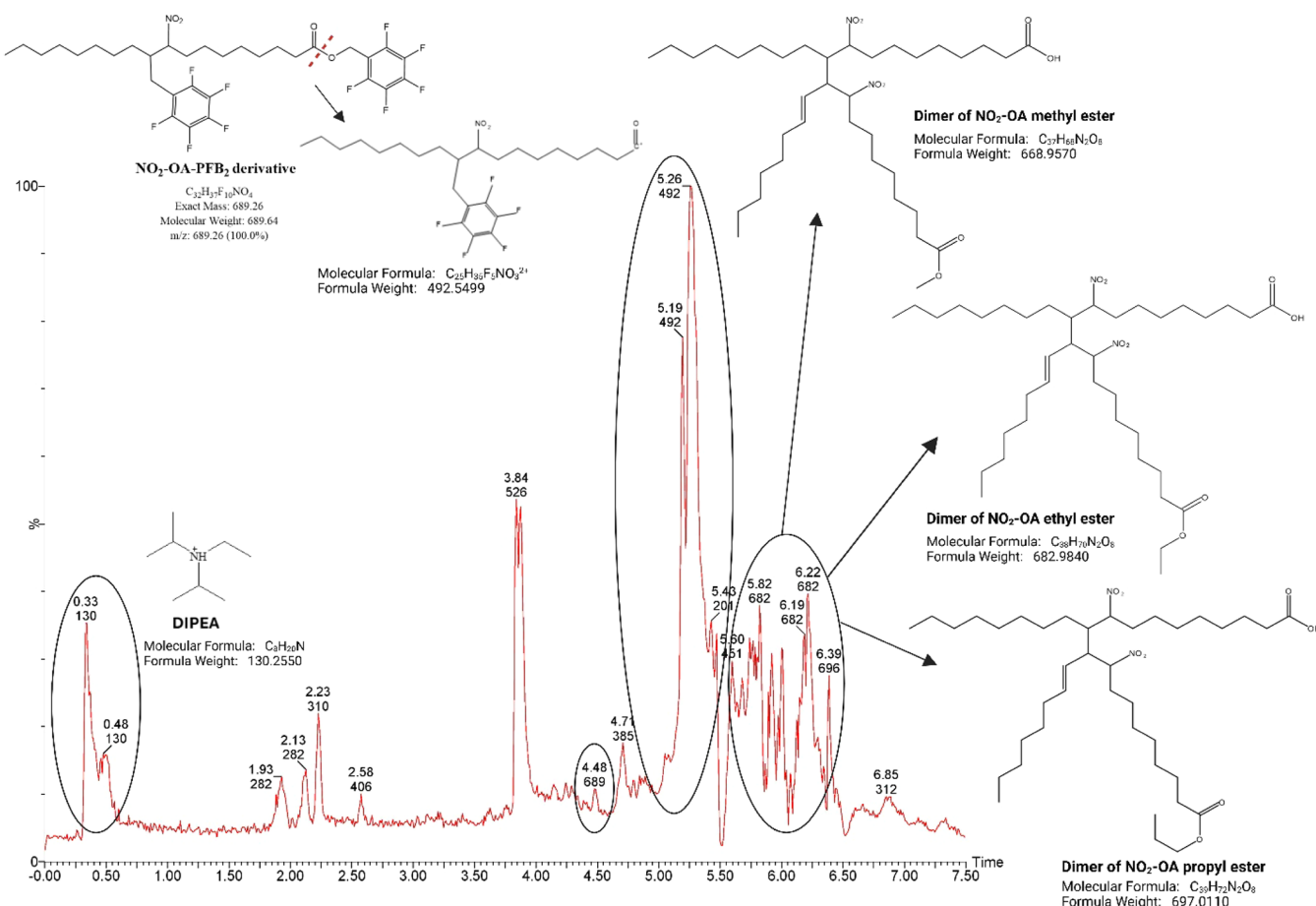


**Figure 7.** Full Scan positive ESI LC-MS/MS of NO<sub>2</sub>-OA after derivatization with the PFB-Br dual-site attacked NO<sub>2</sub>-OA peak ( $m/z$  689) appears at 4.48 min.

proposed dual-site attack mechanism.<sup>30</sup> The formation and stability of this novel dibenzylated NO<sub>2</sub>-OA derivative under our analytical setup are further supported by the consistent linearity observed for the  $m/z$  689 > 327 transition.<sup>9,16</sup>

**Confirmation of NO<sub>2</sub>-OA-(PFB)<sub>2</sub> Formation by LC-MS/MS.** To further confirm the formation of the dibenzylated NO<sub>2</sub>-OA derivative with the predicted fragmentation, an LC-MS/MS run was conducted showing a peak for the dual-site attacked NO<sub>2</sub>-OA at 4.48 min with parent and daughter ions  $m/z$  of 689 and 327, respectively. Figures 7 and 8 support our hypothesis. It is possible that the peak exhibiting the highest intensity at 5.26 min with  $m/z$  492 results from the loss of the PFB-O- group within the column in view of the well-established susceptibility of derivatized products to hydrolysis in the presence of an aqueous mobile phase, resulting in their decomposition.<sup>31</sup> This is consistent with the observation of the small peak ( $m/z$  = 492) at a later retention time, following peaks of higher molecular weights. The peaks at 5.74, 5.82, and 6.39 min, with  $m/z$  values of 668, 682, and 696, respectively, are identified as NO<sub>2</sub>-OA dimers with methyl, ethyl, and propyl esters, respectively. Previous reports indicate that the polarity of the mobile phase and the temperature of the ion source influence the oligomerization of NO<sub>2</sub>-FAs, resulting in the formation of dimers and trimers of NO<sub>2</sub>-OA by a Michael addition reaction mechanism.<sup>9,16</sup>

**Linearity Test of NO<sub>2</sub>-OA-(PFB)<sub>2</sub> Derivative.** Linearity of the GC-MS/MS method for NO<sub>2</sub>-OA (PFB)<sub>2</sub> in methanol was evaluated over the range of 305 nM–30534 nM. Five

calibration solutions were prepared in triplicates and spiked with 5  $\mu$ g/mL of the IS (Figure 9). A linear response was observed for the selected MRM transition 689 > 327, with an  $R^2$  value of 0.9408 and  $p < 0.01$ .

**Extraction and Derivatization of Plasma Samples.** Extraction of plasma was necessary to eliminate proteins and undesirable nonlipid molecules and increase the S/N of target analytes. It includes deproteinization with acidified methanol followed by single-phase extraction adapted from Herz et al.<sup>17</sup> with some modifications namely (a) increasing the volume of plasma (250  $\mu$ L) to achieve better S/N; (b) using 17-BrHDA as the internal standard instead of HDA; (c) deproteinization using MeOH acidified with 20% (v/v) acetic acid instead of 15% for a better protein precipitation. The derivatization reaction was carried out prior to GC-MS/MS analysis to improve volatility, thermal stability, and ionization.<sup>32</sup> The derivatization protocol that was followed in this study is adapted from Tsikas et al.<sup>25</sup> with some modifications to enhance the dual-site attack of NO<sub>2</sub>-OA by PFB-Br, and the subsequent detection of low plasma levels. Critical process parameters influencing the dual-site attack of NO<sub>2</sub>-OA include the reagent to analyte ratio, reaction time, and temperature.<sup>31</sup> Accordingly, the extracted residue was treated with the catalyst 20  $\mu$ L of DIPEA and 20  $\mu$ L of PFB-Br (30% vol. in ACN), which are dual-site volumes used in the literature. In addition, the reaction time was extended to an additional 30 min at 35 °C to ensure the stability of the dual-site attacked NO<sub>2</sub>-OA after the original 1 h at 30 °C.

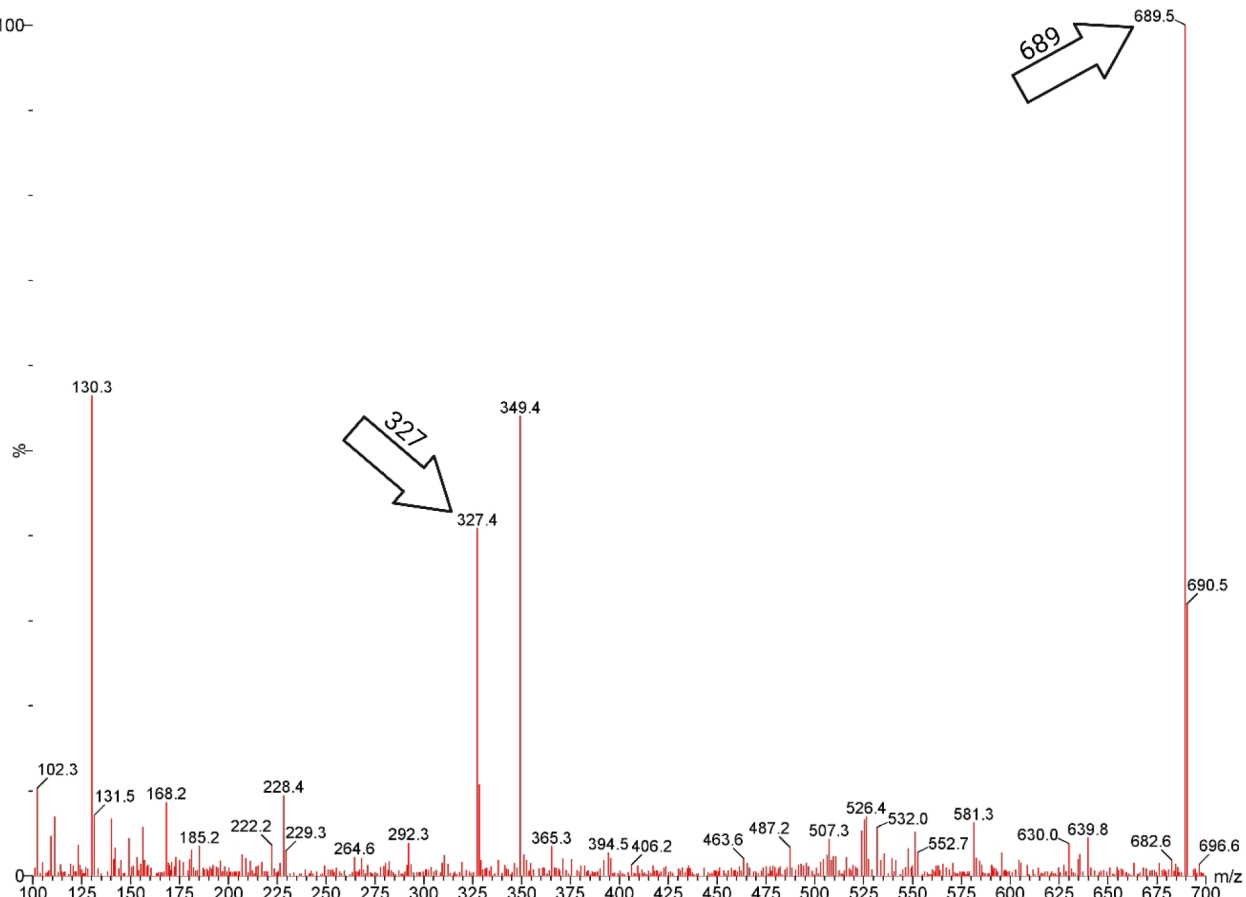


**Figure 8.** LC-MS spectrum of  $\text{NO}_2\text{-OA-(PFB)}_2$  eluting at 4.48 min with the parent ion at  $m/z$  689 and a fragment ion at  $m/z$  327.

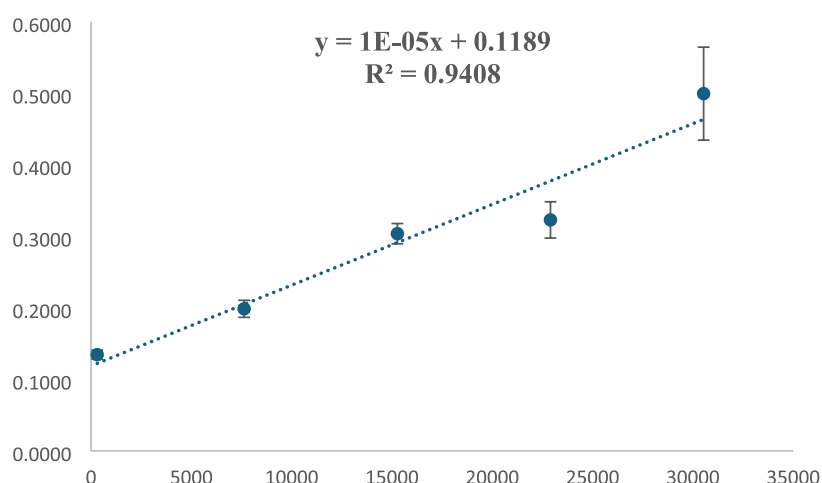


**Figure 9.** Linearity results of  $\text{NO}_2\text{-OA-(PFB)}_2$  in methanol determined by GC-MS/MS.

Our approach achieved a good limit of detection (LOD) and limit of quantification (LOQ). The LOQ of a concentration of 305 nM  $\text{NO}_2\text{-OA-(PFB)}_2$  produced an S/N of 60.2 (Figure 10A). This indicates a possible LOQ of 50 nM for  $\text{NO}_2\text{-OA-(PFB)}_2$  (S/N 10:1) in plasma by utilizing our method. Reported endogenous plasma concentrations of  $\text{NO}_2\text{-OA}$  are approximately 21 nM in patients with ischemic heart disease (IHD) and 12 nM in healthy individuals.<sup>16,17</sup> Consequently, although the S/N of the endogenous  $\text{NO}_2\text{-OA-(PFB)}_2$  peak in plasma was determined to be 4.1 (Figure 10B), demonstrating that detection is possible, these values remain

below our defined limit of quantification (50 nM). Hence, our method allows detection rather than quantification of endogenous  $\text{NO}_2\text{-OA}$  levels in plasma in view of the reported physiological levels in the literature.

**Comparison of  $\text{NO}_2\text{-OA}$  in Plasma Samples of Patients and Controls.** The internal standard 17-BrHDA was spiked into all study samples to a final concentration of 5  $\mu\text{g}/\text{mL}$ . Sample extraction and analysis order were randomized to avoid a systematic bias. The targeted study was carried out on 15 AMI patients and 15 healthy controls (Table S). Since our method allows a good LOD rather than LOQ, the peak

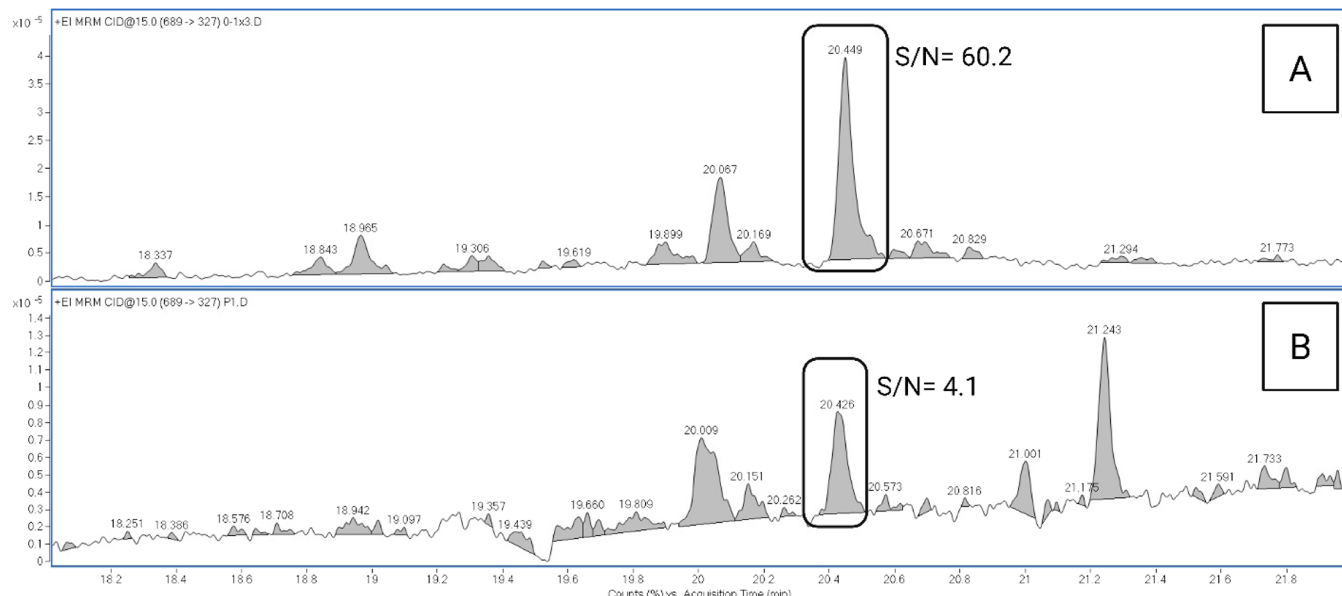


**Figure 10.** GC-MS/MS Detection of  $\text{NO}_2\text{-OA-(PFB)}_2$  in MeOH (A) and plasma (B).

area ratios were used to compare  $\text{NO}_2\text{-OA}$  levels in AMI patients and healthy controls.

**Table 5. Endogenous  $\text{NO}_2\text{-OA}$  in AMI Patients and Healthy Controls Plasma Samples**

Group	$\text{NO}_2\text{-OA}$ peak area ratio (mean $\pm$ SD)	Shapiro-Wilk test for normality	Comparison ( <i>t</i> -test)
AMI patients	$0.0012 \pm 0.0008$	$P = 0.1375$	$P = 0.0039$
Healthy controls	$0.0004 \pm 0.0002$	$P = 0.8098$	

Analysis revealed that the mean peak area ratios of  $\text{NO}_2\text{-OA}$  were higher in patients than controls (Table 5). To test the significance of these results, the Shapiro-Wilk test for

normality was first performed. The obtained *p*-values for both patient and control groups  $>0.05$  (Table 5), suggesting that the data are normally distributed. Accordingly, a parametric Student *t*-test was used to test for significant differences between both groups. Upon excluding outliers determined using the interquartile range (IQR) approach, the statistical analysis produced a *p*-value of 0.0039, indicating an elevated level in  $\text{NO}_2\text{-OA}$  in AMI patients compared to healthy controls (Figure 11).

Numerous animal studies have shown that after ischemia-reperfusion (I/R) and ischemic preconditioning (IPC) events, activated inflammatory cells in both heart tissue and mitochondria produce  $\text{NO}_2\text{-FAs}$  at high nanomolar concentrations.<sup>33,34</sup> Elevated rates of RNS formation, an acidic pH, and an apparent increase in ROS development are character-

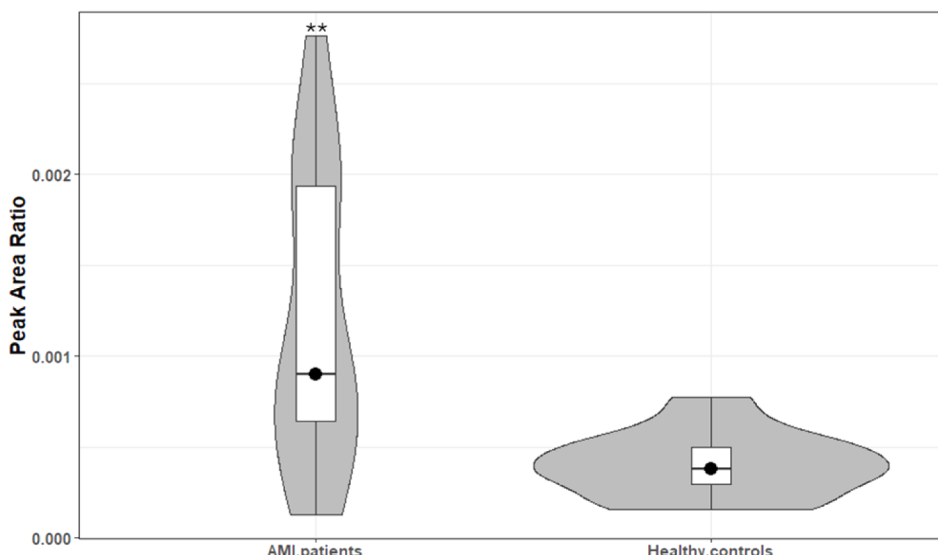


**Figure 11.**  $\text{NO}_2\text{-OA}$  levels in AMI patients and healthy controls are represented as peak area ratios. The white box represents the interquartile range, the black dot represents the median of values, and the gray part represents the overall distribution of the values including the minimum and maximum observations.

istics shared by both *I/R* and IPC. Through the nitration of fatty acids mediated by free radicals, which is facilitated by an acidic pH, this environment encourages the synthesis of NO<sub>2</sub>-FAs.<sup>35</sup> Free radical-mediated nitration of FAs preferentially occurs under low oxygen conditions, where nitroalkenes are easily formed. Conversely, in the presence of oxygen, unsaturated keto derivatives are formed. This insight further explains the detection of NO<sub>2</sub>-FAs in ischemic hearts.<sup>35</sup> Moreover, the liberation of NO<sub>2</sub>-FAs from their protein adducts was evidenced *in vitro* under nitro-oxidative conditions.<sup>36</sup> Specifically, previous findings emphasized that H<sub>2</sub>O<sub>2</sub> and ONOO<sup>-</sup>, as markers of ROS and RNS generated under stress conditions, can oxidize cysteine-adducted NO<sub>2</sub>-FAs, resulting in the release of free nitroalkenes. The release may partially account for the observed rise in the NO<sub>2</sub>-FA content under various stress events.

In the context of these observations, together with the markedly elevated levels of NO<sub>2</sub>-OA, we noted that the increase in NO<sub>2</sub>-OA in AMI patients may result from the nitration of unsaturated fatty acids under stress or from its release from protein adducts. Herz et al. previously reported similar findings, having developed and validated an LC-MS/MS method for the endogenous quantification of NO<sub>2</sub>-OA levels, which were significantly elevated in patients with IHD ( $21.7 \pm 9.8$  nM) compared to healthy controls ( $12.6 \pm 6$  nM), with a *p*-value < 0.01. Nevertheless, an evaluation of NO<sub>2</sub>-LA levels revealed no significant differences across those groups.<sup>16,17</sup> It is possible to speculate that NO<sub>2</sub>-OA may have leaked from disrupted cardiac cells or generated in the vascular compartment. It is important to note that our study samples were taken 2–3 h after the onset of chest discomfort. This duration is significantly shorter than the common period for assessment of other presently utilized biomarkers for myocardial infarction, which are not possibly identifiable until a minimum of 4–6 h after myocardial damage, by which point the condition is already in an irreversible phase. Our data indicate that NO<sub>2</sub>-OA may demonstrate early changes during ischemia episodes; nevertheless, we acknowledge that this observation is preliminary. Additional research with larger cohorts and further validation is necessary to ascertain whether NO<sub>2</sub>-OA could aid, together with other preliminary metabolic indicators, in the early detection of ischemic heart diseases.<sup>37</sup>

**Targeted Method Limitations.** The limited cohort size ( $n = 15$ ) constitutes a constraint when accounting for the intrinsic biological heterogeneity of cardiovascular disease groups. This number was established as a priori through G-power analysis to guarantee enough statistical power based on previously documented effect sizes. The individuals were meticulously chosen to reduce confounding variables and biological variability, especially as no food restrictions were enforced in this study. This regulated method attempted to minimize irrelevant sources of variation that might conceal authentic metabolic variations. Larger cohorts may improve generalizability, but they also increase the risk of including participants with more comorbidities or uncontrolled variables that could obscure interpretation. Considering its limited size, the cohort produced reproducible and consistent metabolic profiles, thus validating the observed patterns and emphasizing the study's function as an analytically oriented, exploratory investigation.

It should be stated that the current approach has several limitations, despite its innovative design and analytical rigor. The use of 17-BrHDA as an internal standard, while cost-

effective and structurally relevant, does not entirely mimic the isotopic and physicochemical features of endogenous NO<sub>2</sub>-FAs, which might lead to minor variations in ionization efficiency and matrix recovery. Moreover, the absence of thorough quantitative validation, such as matrix spike recovery, inter- and intraday precision, and isotope dilution experiments, indicates the exploratory rather than clinical emphasis of this study. The comparatively large LOQ (~50 nM), above physiological values, hinders its direct application to absolute quantification in biological samples. Nonetheless, the method substantially expands the field by presenting an innovative derivatization technique and illustrating the viability of employing 17-BrHDA as a practical substitute for isotope-labeled standards. As such, it provides a valuable foundation for future refinement and adaptation toward fully validated quantitative applications.

### Untargeted Metabolomics Study

Untargeted metabolomic analysis was performed to explore similarities and differences in the metabolome profiles of the studied groups.

### GC-MS for Untargeted Metabolomic Analysis

Trimethylsilylation approach and its variants are the most common derivatization protocols, while alkylation and acylation are less used in GC-MS-based metabolomics.<sup>5</sup> Limiting derivatization to one type is experimentally more convenient for routine analysis, yet it prevents the ability to detect different classes of compounds in good sensitivity. Hence, to achieve a comprehensive coverage of metabolites, our untargeted study employed two derivatization reactions: alkylation and silylation. In the latter, trimethylsilyl (TMS) groups substitute the active proton in a variety of functional groups including OH, COOH, SH, NH, CONH, POH, and SOH. In this study, *N*-Methyl-*N*-(trimethylsilyl)-trifluoroacetamide (MSTFA) was the silylation reagent of choice because it is the most volatile, mild, and versatile trimethylsilylacetamide reagent and hence appropriate for complex metabolites in blood.<sup>5</sup> Alkylation is conceptually comparable to silylation, since both processes include the nucleophilic replacement of active hydrogens. However, alkylated derivatives can be isolated and "preserved" if needed because they are not only less polar but more stable than the analog silylated derivatives that readily hydrolyze in the presence of trace levels of water. Phenols, thiols, and carboxylic acids were alkylated by 2,3,4,5,6-pentafluorobenzyl bromide (PFB-Br)<sup>31</sup> under a flexible range of pH reaction conditions, which is experimentally convenient. In our study, we found that fatty acid chains in the alkylated form have better sensitivity than the silylated ones (Figure 4). Consequently, PFB-Br was selected as the derivatization reagent for alkylation in the untargeted approach.

### Multivariate Data Analysis

Owing to the complexity of the acquired data and considering the large number of samples and monitored metabolites, multivariate data analysis was performed via supervised and unsupervised methods. Unsupervised analysis using PCA identifies patterns within the data without considering the type or class of the study samples, while supervised methods (PLS-DA) identify patterns within the data that are correlated with the phenotypic variable of interest by building a regression model, while down-weighting other sources of variance.<sup>38</sup>

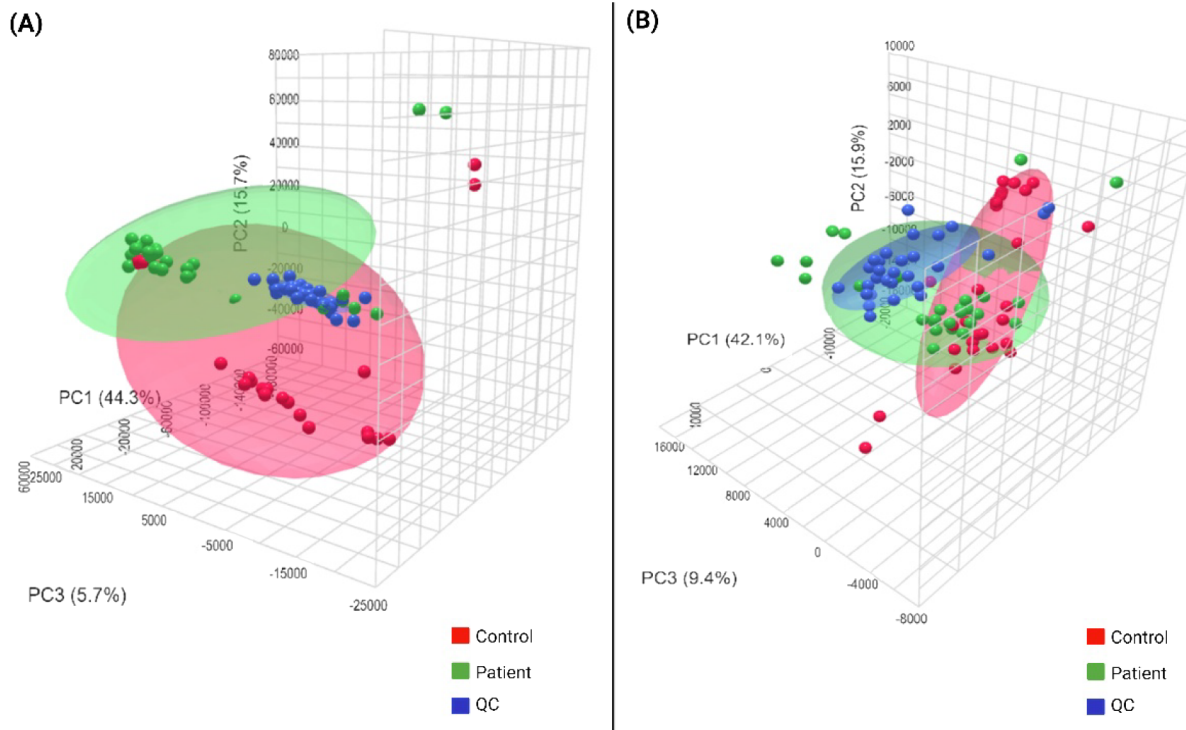


**Figure 12.** 3D PCA score plots of patients and controls obtained from normalized silylated (A) and alkylated (B) samples' data.

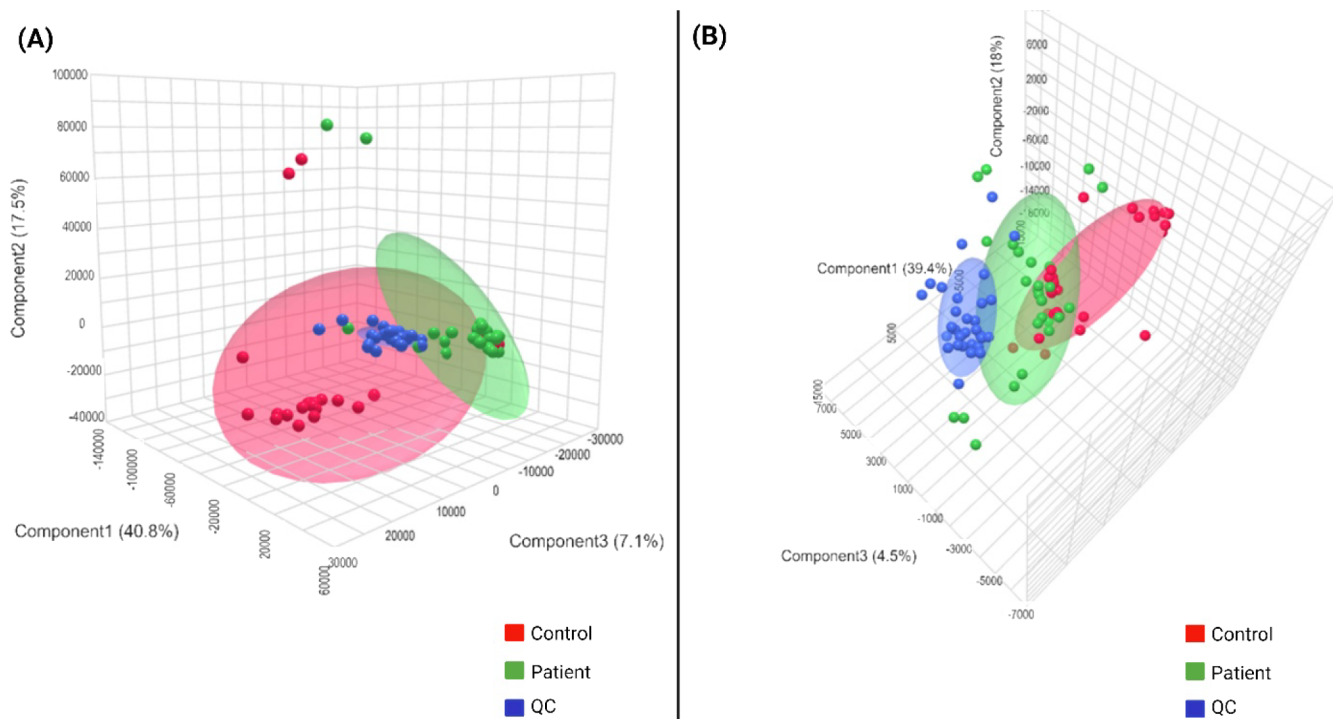


**Figure 13.** 3D PLS-DA score plots of patients and controls obtained from normalized silylated (A) and alkylated (B) samples' data.

**Principal Component Analysis (PCA).** PCA was first applied to the acquired chromatographic and mass spectral data on silylated and alkylated samples, separately. The 2D score plot obtained for the silylated samples' data showed two distinct clusters for AMI patients and controls. The first two components of the PCA score plot were responsible for 60% of the total variance of the metabolic profile being able to discriminate between the two groups (Figure 12A). A previous

study on the plasma of STEMI patients and healthy controls using GC-MS reported that the variance between the data was explained by 42% and 16% along PC1 and PC2, respectively,<sup>39</sup> which is close to our results. For alkylated samples, the 2-D score plot showed a slight discrimination between the AMI patients and healthy controls, with a total variance of 57.5% (Figure 12B). Hence, Alkylation showed a difference between the two groups, close but not as discriminant as silylation in

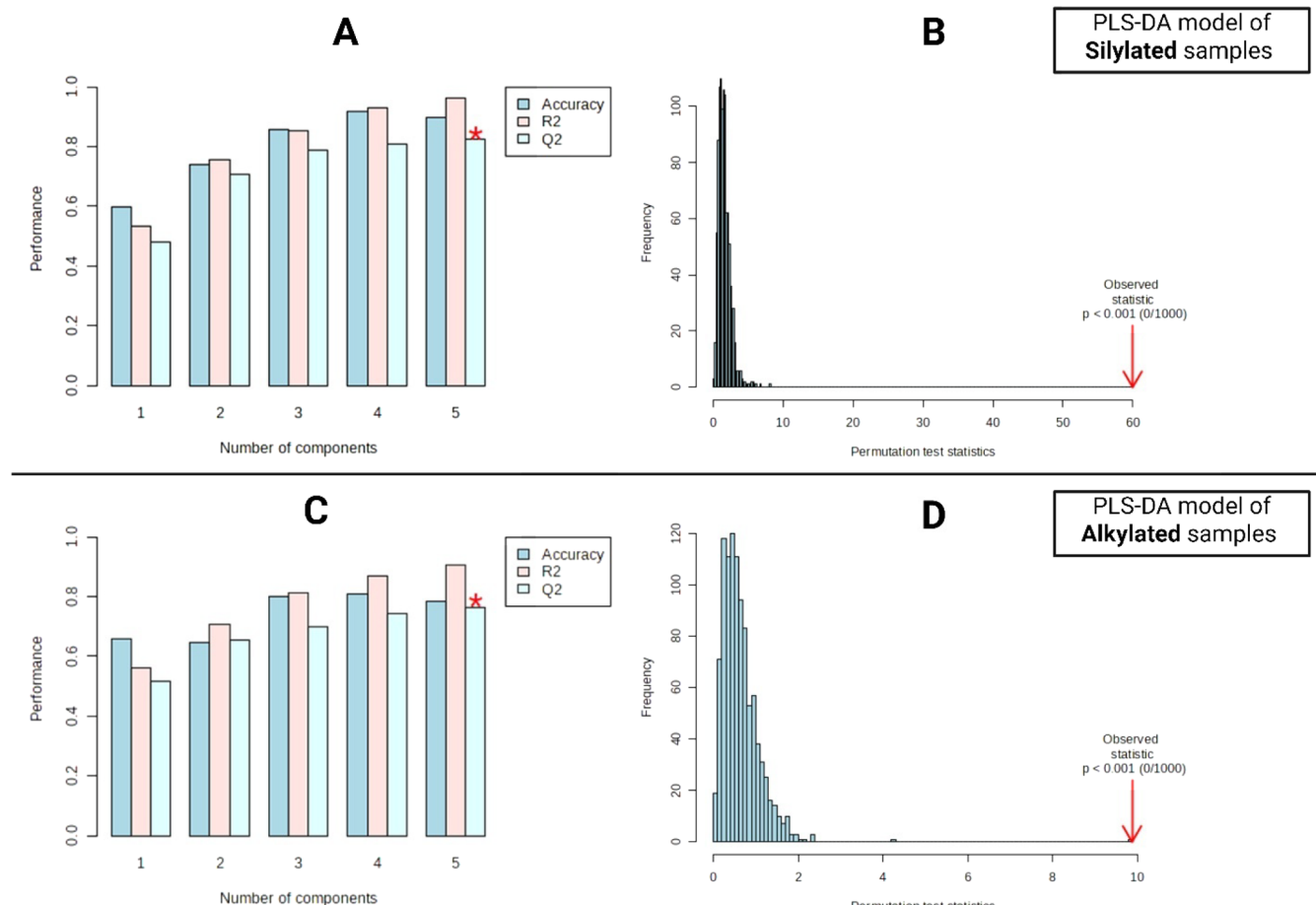


**Figure 14.** (A) Cross-validation results of the PLS-DA model for silylated samples showing the model performance as a function of the number of components. Deep blue bars represent classification accuracy, pink bars represent  $R^2$  (explained variance), and light blue bars represent  $Q^2$  (predictive ability). The optimal number of components selected for the model is indicated by a red asterisk. (B) Permutation test ( $n = 1000$ ) was used for the PLS-DA model of silylated samples. The observed test statistics (red arrow) is significantly higher than those obtained from permuted class labels, yielding  $p < 0.001$  (0/1000), confirming the robustness and validity of the model. (C) Cross-validation results of the PLS-DA model for alkylated samples, displaying accuracy,  $R^2$ , and  $Q^2$  values across increasing numbers of components, with the optimal model indicated by a red asterisk. (D) Permutation test ( $n = 1000$ ) for the PLS-DA model of alkylated samples, showing a statistically significant separation between observed and permuted models ( $p < 0.001$ , 0/1000), demonstrating strong model reliability.

this study or reported literature.<sup>39</sup> Our study is novel in being the first to use an alkylation-based GC-MS metabolomics study on AMI patients emphasizing the contribution of carboxylic acids in AMI conditions (Figure 4). QC samples were perfectly clustered, showing the accuracy of our analysis and that the discrimination between samples was due to biological variability, not technical variability (Figure 12).

**Partial Least-Squares Discriminant Analysis (PLS-DA).** PLS-DA is a supervised technique for classification by incorporating class labels to enhance the model's ability to discriminate between different categories. PLS-DA not only reduces dimensionality but also aims to maximize the separation between predefined classes, making it particularly useful for the goal of predicting categorical outcomes based on input features. Together, PCA and PLS-DA offer powerful tools for analyzing and interpreting high-dimensional data, where PCA provides insights into data structure and variance, while PLS-DA facilitates classification and predictive modeling.<sup>40</sup>

To further verify clustering, PLS-DA was applied to identify metabolomic patterns that are correlated with each class of the study samples. The obtained PLS-DA score plots showed clear

discrimination between the data of AMI patients and controls obtained from both derivatization reactions (Figure 13).

Validation of the PLS-DA models presented high  $R^2$  and  $Q^2 > 0.5$  for all the 5 components (latent variables) indicating high reliability and predictability of the model. Cross-validation tests were performed for both models using 5-fold cross-validation (CV) with  $Q^2$  as a measure of performance, where it represents an estimation of the model's predictive capability computed by cross-validation (CV). In each cross-validation, predicted data were compared to original data, and the sum of squared errors was computed. The prediction error was subsequently aggregated over all samples, termed the Predicted Residual Sum of Squares (PRESS). For convenience, the PRESS was normalized by the starting total of squares and subtracted from 1 to align with the scale of  $R^2$ . Accurate projections exhibit low PRESS or high  $Q^2$  values, where a negative  $Q^2$  indicates that the model lacks predictive capability or is overfitted,<sup>41</sup> while  $Q^2 = 0.99$  may be perceived as indicative of robust models with significant discriminative ability, such diagnostic statistics can be achieved merely by chance through a fortunate selection of samples in the test, validation, and training sets.<sup>42</sup> To address these issues and to

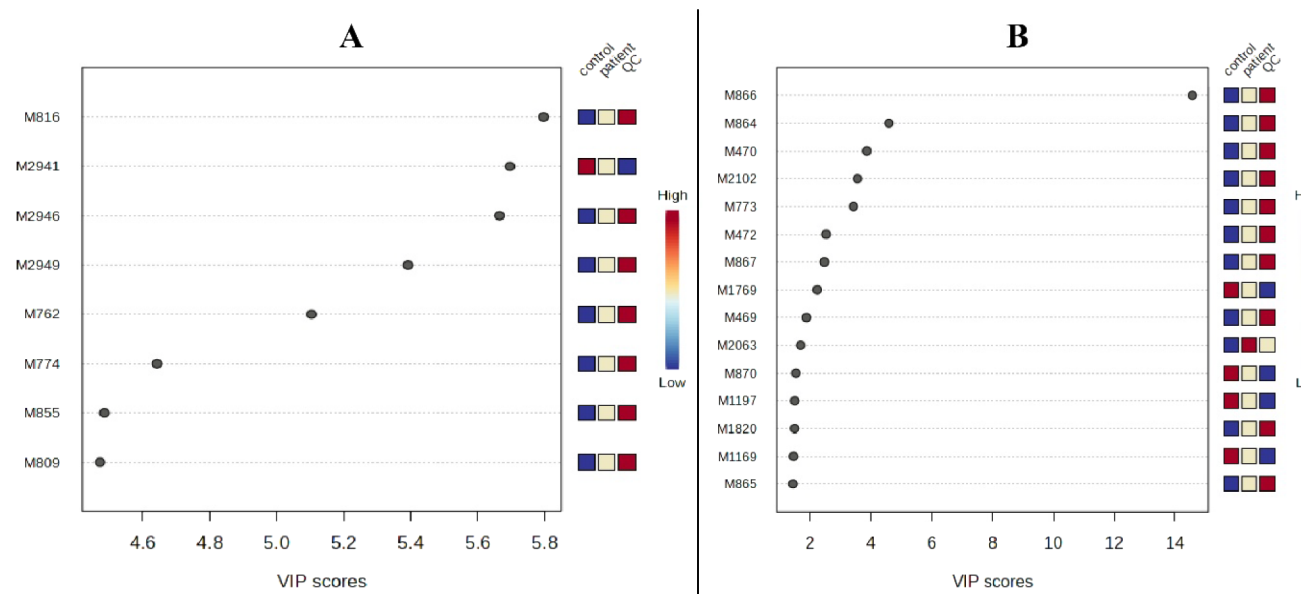


**Figure 15.** VIP scores of the top 8 important features identified by the PLS-DA model of silylated samples (A); and the top 15 important features identified by the PLS-DA model of alkylated samples (B).

**Table 6. Characterized VIP Features Obtained from the Silylated Samples Using HMDB**

VIP	Rt (min)	Metabolite	Experimental RI	Library RI	FDR	Levels in AMI patients
M816	10.43	Fumaric acid	1243	1328	9.276621e-12	↑
M2941	21.52	Serine methyl ester	1226	1135	1.568464e-08	↓
M762	10.19	(2R)-3-Sulfanylpropane-1,2-diol (thioglycerol)	1237	1348	7.469746e-07	↑
M855	10.68	Acetylglycine (Ac-Gly)	1249	1304	4.532188e-13	↑
M809	10.39	D-Pipecolic acid	1242	1261	2.967026e-12	↑

quantify the statistical significance of the diagnostic statistics (*p*-value), a permutation test was implemented<sup>43,44</sup> to test the distinction between the two randomly constituted groups.<sup>45</sup> In the permutation test, sample labels were randomly rearranged, and a new classification model was computed.<sup>43</sup> A relatively large sample size was necessary to accurately determine the empirical *p*-values; hence, we estimated the sample size using G-power to allow permutation testing for both PLS-DA models. Hence, 1000 permutations were used to validate the model showing *p* < 0.001 for the silylated and alkylated samples (Figure 14) meaning that out of 1000 permutations, none of the resulting models achieved a separation distance as large as the one observed with the actual data. In conclusion, the permutation test results strongly support the validity of the PLS-DA models, where a low *p*-value indicates that the observed separation between the classes is unlikely to have occurred by chance, suggesting that both models are indeed capturing a real and significant relationship between the measurements and the class memberships.

**Variable Importance in Projections (VIPs).** PLS-DA provides Variable Importance in Projection (VIP) scores, which discriminate metabolites responsible for the separation observed. For the silylated samples, the top 8 features with the highest VIP scores were displayed (Figure 15). Whereas for the alkylated samples, 15 features were displayed to further investigate what the alkylation reaction can uncover (Figure 15). The metabolites that were selected as possible biomarkers had VIP score >1 based on the results of the PLS-DA model.<sup>46</sup> Notably, NO<sub>2</sub>-OA was not among those VIP features and was not detected in the untargeted analysis due to the low

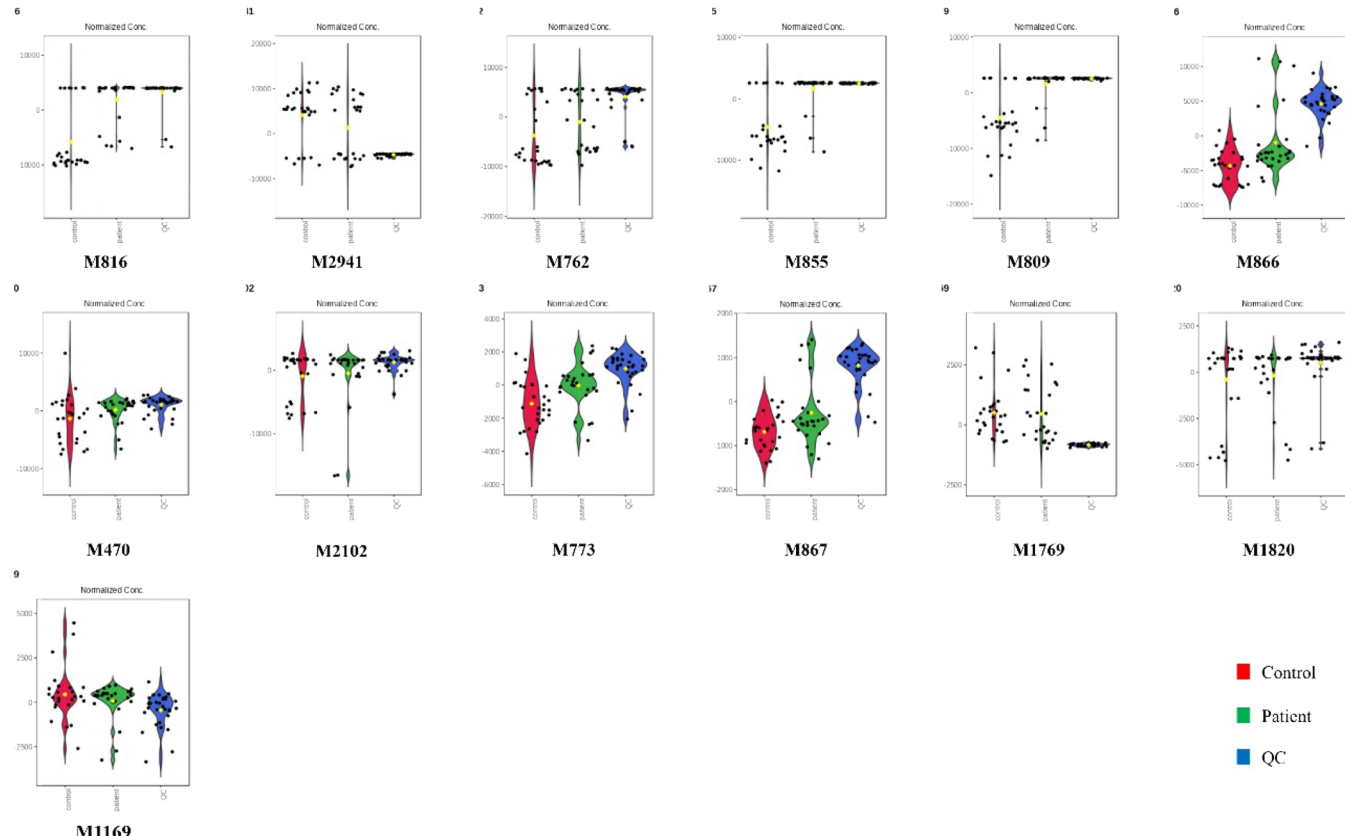
sensitivity to NO<sub>2</sub>-FAs detection when full-scan mass spectrometric mode was applied. Although NO<sub>2</sub>-OA is a biologically significant metabolite and was found at elevated levels in patients, it did not serve as a principal discriminant between the patient and control groups in our multivariate analysis. This result illustrates the fundamental characteristic of the untargeted metabolomic approach, which aims to encompass the entire metabolic landscape instead of focusing on certain predetermined targets. The aim of this investigation was not to measure or validate established biomarkers but to uncover unforeseen or secondary compounds which promote group differentiation. The lack of NO<sub>2</sub>-OA among the primary discriminant traits does not undermine the analytical significance of the untargeted workflow; instead, it emphasizes its exploratory capability in revealing new metabolic changes outside of recognized targets.

#### Annotation of Metabolites Obtained from VIP Score Plots

The difficulty of metabolite identification in untargeted metabolomics is related to incomplete spectrum libraries and inadequately defined human metabolomes, which require effective annotation methodologies. In accordance with the Metabolomics Standards Initiative (MSI) guidelines, our annotation process emphasized putative identification, namely, “putatively characterized compound class” and “putatively annotated compounds” via comparison of experimental EI mass spectra with the Human Metabolome Database (HMDB). We enhance the reliability of our proposed identification by additional approaches to spectral similarity.<sup>18</sup> We utilized the retention index considering the GC column type as semistandard nonpolar and the type of derivatization

**Table 7. Characterized VIP Features Obtained from the Alkylated Samples Using HMDB**

VIP	Rt (min)	Metabolite	Experimental RI	Library RI	FDR	Levels in AMI patients
M866	18.471	3,4-dihydroxybutyric acid	1641.24	1799.674	1.907434e-15	↑
M470	10.678	Malonic acid	1248.65	1369.0242	7.006463e-03	↑
M2102	32.816	Oleic acid	2612.79	2477.4001	5.689952e-02	↑
M773	16.058	Homocysteine	1678.06	1605.7001	8.507555e-08	↑
M867	18.473	3-Hexenedioic acid	1641.30	1677.5677	4.692342e-16	↑
M1769	29.725	L-beta-aspartyl-L-aspartic acid	2294.12	2494.8828	5.453295e-08	↓
M1820	30.262	Carnosine	2414.19	2587.985	1.069934e-01	↑
M1169	22.354	2-Octenedioic acid	1851.09	1911.3542	2.085510e-02	↓

**Figure 16.** Violin plot of each annotated VIP showing their normalized concentrations across different sample types.

method (silylation or alkylation). This comprehensive technique exploits the intrinsic consistency and distinctive fragmentation patterns provided by EI ionization,<sup>18</sup> facilitating assertive structural conclusions.

By employing these rigorous criteria on our data, we effectively annotated five of the principal VIP features from the silylated samples (Table 6) and eight from the alkylated samples (Table 7).

The combination of spectral similarity with chromatographic retention data and experimental context enabled us to surpass fundamental database matching, yielding a more dependable characterization of the metabolites that most significantly influenced the observed variance among patients and controls.

In Figure 16, metabolites exhibiting narrow and high violin plots indicate a more uniform level of importance in differentiating between sample groups. Those are M816, M2941, M762, M855, M809, M1769, and M1820. In contrast, metabolites with wider, flatter violin plots indicate a greater degree of variability in their importance depending on the component being examined, such as M866, M470, M2102,

M773, M867, and M1169. Determining whether a metabolite's significance is stable or fluctuating can offer insights into the fundamental biological systems. A consistently significant metabolite may be associated with a basic distinction between the groups, whereas a variably significant one may be connected to more specific or secondary effects.

#### Pathway Reconstruction for Understanding Metabolite Links to Cardiovascular Diseases

In this study, samples were collected from AMI patients at the triage and prior to being admitted to the intensive care unit. Blood samples were collected before any medicine was administered, where inadequate blood flow and resulting in a stress response can alter the overall metabolism.

Concerning the interpretation of metabolite pathways, it is worth mentioning that the annotation relied on retention index (RI), mass spectral similarity, and column type, but was not validated using authenticated standards. To enhance biological relevance, current literature was utilized to support the postulated correlations and direct future inquiries.

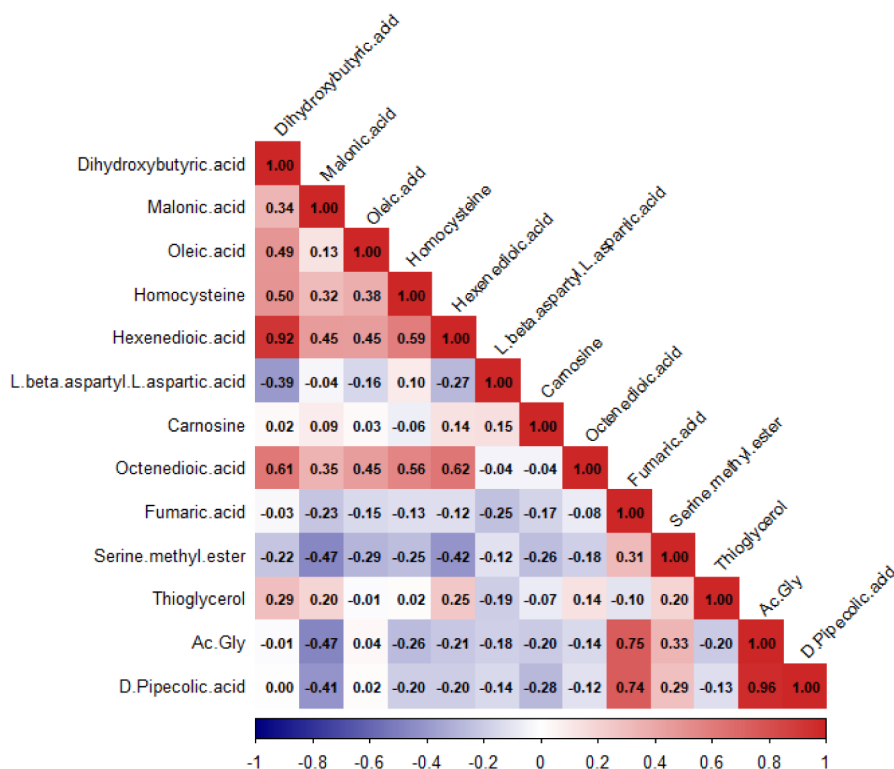


**Figure 17.** Correlation plot of annotated VIPs recognized in AMI patients.

Cardiac troponins can be detectable within 4–6 h from the first episode of myocardial damage, indicating that the condition has progressed to an irreversible stage.<sup>47</sup> The metabolic changes seen in this study were clear at the time of diagnosis, which may be advantageous for diagnosing myocardial infarction, particularly for individuals who are troponin-negative upon admission.

Oxidative stress and ischemia-induced changes in energy metabolism, amino acid metabolism, fatty acid oxidation, anaerobic glycolysis, urea cycle, and pathways associated with endogenous gasotransmitters are the main identified altered metabolic pathways.<sup>39</sup> Particularly if troponin values are negative upon hospital admission, which might occur in silent AMI patients, these metabolic alterations may be helpful for early risk diagnosis in MI patients. We were able to identify specific groups of related metabolites that show coordinated reactions to ischemia and hold significant promise for the early detection of AMI patients by employing such a comparative metabolomics approach.

Our data indicate that ischemia serves as the primary factor influencing cellular metabolism to adjust to oxygen shortage and sustain metabolic activity. Ischemic stress is linked to increased hydrocortisone levels, which can frequently impair insulin sensitivity. Insulin resistance in adipose tissue impairs the insulin signaling cascade's capacity to retain lipids. This stimulates lipolysis and diminishes lipogenesis.

### Oleic Acid

In accordance with this idea, our findings show increased glycerol concentrations, and free fatty acids such as oleic acid in the blood of AMI patients, consistent with previous reports.<sup>48–50</sup> According to the literature and our findings, oleic acid emerged as a significant variable of importance in projection (VIP) according to its unadjusted *p*-value (*p* < 0.05). Nonetheless, upon implementing multiple-testing

correction, the adjusted *p*-value (FDR) revealed that oleic acid was not statistically significant. This disparity emphasizes the essential requirement to analyze multivariate outcomes with false discovery rate-adjusted data. Despite oleic acid being classified as a prominent discriminant metabolite by VIP, its insignificance following FDR correction implies that its discriminatory potential should be regarded with caution. This emphasizes the necessity of preferring FDR-adjusted outcomes above unadjusted *p*-values when deriving biological inferences from high-dimensional metabolomic data sets.

### 2-Octenedioic Acid

We also found decreased medium-chain fatty acids like 2-octenedioic acid with a statistically significant (*p*-value < 0.01) and positive monotonic correlation between the levels of oleic acid and octenedioic acid.<sup>51</sup>

### Thioglycerol

As for thioglycerol, despite being a sulfur-containing derivative of glycerol, it is not commonly recognized as a major endogenous metabolite in the human biochemical pathways. While there is no direct, well-documented, endogenous pathway for thioglycerol biosynthesis, thiol-containing compounds such as glutathione, cysteine, and homocysteine may interact with glycerol intermediates. We hypothesize that glycerol or its derivatives (e.g., glyceraldehyde-3-phosphate or dihydroxyacetone phosphate) could undergo a sulfhydrylation reaction involving hydrogen sulfide (H<sub>2</sub>S) or thiol groups from cysteine or glutathione which were reported to be elevated in AMI patients.<sup>39</sup> The correlation plot (Figure 17) indicates that this observation is not directly associated with any of the annotated VIPs, suggesting that its increase may have resulted from secondary effects, permitting the proposal of our hypothesis.

## Homocysteine

Increased total homocysteine levels were reported to cause oxidative damage to vascular endothelial cells and hinder nitric oxide synthesis, a potent vasodilator, in the endothelium.<sup>52–54</sup> Hyperhomocysteinemia increases platelet adhesion to endothelial cells and stimulates the proliferation of vascular smooth muscle cells.<sup>53,55</sup> This escalates the progression of coronary artery occlusion recognized in AMI patients.

## Carnosine

Furthermore, muscle carnosine levels were found to be negatively associated with insulin sensitivity. This indicates that elevated carnosine levels may serve as an adaptive mechanism to mitigate chronic inflammation and oxidative stress associated with obesity, insulin resistance, and diabetes. This pathophysiological model resembles hyperinsulinemia, which arises as a consequence of insulin resistance. Proposed pathways by which carnosine influences glucose metabolism comprise anti-inflammatory and antioxidant actions. It can be hypothesized that carnosine may function as a physiological substrate in some metabolic pathways, the disruption of which could lead to diminished carnosine consumption and subsequent accumulation as supported by our results.<sup>56</sup> A similar outcome was noted for carnosine, which demonstrated a high VIP score but lost significance following the FDR adjustment. This further demonstrates that VIP measures alone may exaggerate the significance of specific compounds in high-dimensional metabolomic data sets. Both oleic acid and carnosine are robustly substantiated by extant research, and their biological significance has been consistently highlighted.<sup>50,51,57</sup> Consequently, despite the conservative approach of FDR correction, we chose to include these metabolites in our findings, as they retain both mechanistic and clinical significance based on external data.

## L-Beta-Aspartyl-L-Aspartic Acid

L-beta-aspartyl-L-aspartic acid is a dipeptide of two amino acids, which are L-aspartic acid.<sup>57</sup> Insulin is an anabolic hormone; hence, insufficient insulin response will lead to a diminished use of amino acids for protein synthesis. A reduction in amino acid availability must result from their utilization as an energy source. Insulin resistance elevates the activity of transaminases, essential enzymes in amino acid metabolic pathways, resulting in recognized alterations in amino acid metabolism in patients, attributed to fluctuations in proteinogenic amino acids such as L-serine and L-aspartate.<sup>51</sup> Thereby, a decrease in the circulating levels of L-aspartate, which serves as a direct precursor for L-beta-aspartyl-L-aspartic acid, would affect the production of this dipeptide, leading to a corresponding reduction in its amounts.

## 3,4-Dihydroxybutyric Acid

A study by Curovic et al. indicates that elevated concentrations of 3,4-dihydroxybutyric acid correlate with an augmented microvascular burden. Elevated levels of this acid may signify damage to the tiny blood vessels.<sup>58</sup> Microvascular dysfunction is pivotal in the onset and advancement of cardiovascular disease, potentially leading to myocardial ischemia despite the lack of substantial obstructions in the major coronary artery specific processes via which 3,4-dihydroxybutyric acid induces microvascular damage that is under investigation. It is believed that this acid may participate in metabolic pathways that lead to oxidative stress and inflammation, both of which could negatively impact the endothelium.<sup>58</sup>

## Malonic Acid

Numerous investigations have revealed increased concentrations of malonic acid in patients with cardiomyopathy. The patients had hypotonia, minor developmental delay, seizures, and cardiomyopathy, accompanied by malonic aciduria and malonyl-CoA decarboxylase insufficiency. Excess malonic acid was observed in the patients while neither feeling ill nor metabolically stressed, reinforcing its capability as a biomarker for cardiovascular diseases, particularly heart failure.<sup>59</sup>

Oxidative stress or hypoxic conditions on cardiac cells produce a metabolomic profile indicative of atherosclerosis, which may facilitate the early detection of acute coronary syndrome (ACS). Numerous studies have indicated the involvement of malonic acids in oxidative stress.<sup>60</sup>

## Fumaric Acid

Fumaric acid is well-known and recognized as an endogenous antioxidant that mitigates oxidative stress.<sup>61</sup> Elevation in malonic acids and reduction in fumaric acid are indicative of oxidative stress in living organisms.<sup>62</sup> In our study, we observed a considerable increase in the amounts of malonic acid, while the levels of fumaric acid were elevated, which is contradictory to its decreased levels reported in an earlier study by Gundogdu et al.<sup>63</sup>

On the contrary, a study on salt-sensitive (SS) hypertensive rats revealed that SS rats had significantly elevated concentrations of five tricarboxylic acid (TCA) cycle-related metabolites: fumarate, succinate, citrate, isocitrate, and *cis*-aconitate.<sup>64</sup> In their research, they discovered that fumarylase (FH), a crucial part of the TCA cycle, was lacking in the kidneys of SS rats. The accumulation of fumarate, its substrate, appears to be more substantiated, consistent with our findings.<sup>65,66</sup> Moreover, a thorough examination of the activity of eight TCA cycle enzymes in the heart, liver, and skeletal muscles provided additional evidence that SS rats had an aberrant TCA cycle. In line with their earlier research on fumarylase in the kidney, several of these enzymes displayed decreased activity in one or more organs examined in SS rats.<sup>66</sup>

The TCA cycle is pivotal in oxidative phosphorylation within the myocardium.<sup>67</sup> The levels of TCA cycle intermediates in cardiomyocytes are meticulously maintained to ensure sufficient production of substrates from glycolysis and the  $\beta$ -oxidation of fatty acids. In acute ischemia, conserving TCA cycle intermediates is crucial for ATP production.<sup>67</sup>

Malonic acid is a competitive inhibitor of succinate dehydrogenase, the principal enzyme in the TCA cycle, which typically facilitates the oxidation of succinate to fumarate. It irreversibly binds to succinate dehydrogenase, hence inhibiting the TCA cycle.<sup>68</sup> Ischemia leads to diminished glucose oxidation, prompting the conversion of pyruvate to lactate to regenerate the NAD<sup>+</sup> required for glycolysis.<sup>69</sup> Our findings indicate that elevated levels of malonic acid inhibit the TCA cycle, thereby conserving its metabolites for ATP synthesis, which leads to increased fumaric acid levels.

## 3-Hexenedioic Acid

3-Hexenedioic acid has been identified as a metabolic biomarker of aging, with elevated levels observed in older adults, especially those with comorbidities like cardiovascular disease, compared to healthy young.<sup>70</sup> It is an unsaturated dicarboxylic acid whose levels increase when fatty acid oxidation is impaired or mobilization is altered. This

compound, derived from the oxidation of long-chain 3-hydroxy dicarboxylic acids, plays a role in cell signaling and membrane stabilization.<sup>71</sup>

Although 3-hexenedioic acid is susceptible to lipid peroxidation, it is less affected by oxidative stress than other similar fatty acids.<sup>70</sup> This feature has not been extensively explored in aging studies and warrants further investigation.

Elevated levels of 3-hexenedioic acid have been associated with suppressed fatty acid oxidation. Additionally, dihydroxybutyric acid, a product of short-chain fatty acid metabolism, may reflect disruptions in the fatty acid pathways. Compromised pathways in the breakdown or utilization of fatty acids may result in the buildup of intermediate or related molecules, demonstrating a strong, significant positive correlation (Figure 17) with  $p$ -value < 0.001.

### Acetylglycine

Glycine is essential for collagen synthesis, and collagen deficiency in the arterial wall was reported to promote calcification of the arterial middle layer.<sup>46,72</sup> Furthermore, glycine can enhance  $\beta$ -oxidation activity by stimulating the PPAR $\gamma$  signaling pathway and possesses antiatherosclerotic and anti-inflammatory characteristics.<sup>73</sup>

In this study, elevated acetylglycine may reflect a reduction in glycine levels, which can suppress PPAR $\gamma$  activity—an indicator of inflammation and oxidative stress.<sup>74</sup>

Glycine and serine are metabolically linked via serine hydroxymethyltransferase (SHMT),<sup>75</sup> which enables the reversible transformation between these amino acids in the one-carbon metabolic pathway. A disruption in glycine metabolism, evidenced by the increased amounts of acetylglycine observed in this study, can subsequently influence serine dynamics by modifying the balance between serine and glycine.

Both serine and glycine exhibit significant sensitivity to metabolic disruptions, including insulin resistance and oxidative stress, thereby illuminating the strong significant positive correlation ( $p$ -value < 0.01) determined between serine and acetylglycine levels.

### D-Pipecolic Acid

Lysine derivatives, D-pipecolic acid and L-pipecolic acid, are enantiomers of one another. L-pipecolic acid has been shown to have a protective impact by converting excess glucose to ATP for energy at the cellular and molecular level through oxidative phosphorylation in hepatocytes.<sup>76</sup> Patients with coronary artery disease (CAD) and type 2 diabetes mellitus (T2DM) who also had CAD showed a negative correlation with L-pipecolic acid.<sup>76</sup> According to earlier research as well, patients with T2DM have a reduced level of pipecolic acid.<sup>77,78</sup>

In contrast, the role of D-pipecolic acid remains poorly understood. However, our study found elevated levels of D-pipecolic acid, suggesting that it may have metabolic relevance. Similarly, Priyadarshini et al. reported higher levels of both D- and L-pipecolic acid in diabetic corneas compared to healthy controls.<sup>79</sup>

We also observed a strong positive correlation ( $p$  < 0.001) between D-pipecolic acid and fumaric acid, possibly due to fumarate accumulation from mitochondrial stress. This may alter amino acid metabolism, particularly lysine degradation, resulting in increased D-pipecolic acid levels.

In summary, untargeted metabolomics represents a major shift in metabolic research—from focusing on specific pathways to exploring complex metabolic networks in a

hypothesis-generating manner.<sup>80</sup> This study identified 13 serum metabolites in AMI patients that may serve as candidate biomarkers for early detection, offering new insights into disease-related metabolic changes. These findings highlight the value of metabolite profiling in uncovering early markers of adverse cardiac events and guiding timely medical intervention.

Further research is needed to understand the clinical significance of these biomarkers and to evaluate their responses to therapeutic interventions.

## CONCLUSION

Our bioanalytical method was the first to utilize 17-BrHDA as an internal standard more robust for measuring endogenous NO<sub>2</sub>-FAs than the formerly used HDA. Additionally, we report for the first time alkylated and silylated mass spectra of 17-BrHDA showing that alkylated long-chain fatty acids have higher GC-MS sensitivity compared to silylated ones in positive ion mode. In EI GC-MS/MS, the well-known low sensitivity to NO<sub>2</sub>-FAs was reversed when their PFB methyl esters were examined. Based on our proposed mechanism, a dual-site attack occurs by the derivatizing reagent PFB-Br, which represents a novel derivative. In contrast to previous methodologies measuring NO<sub>2</sub>-FAs in biological matrices, this work is the first comparative study for detecting NO<sub>2</sub>-FAs in humans and assessing their levels with and without IHDs by EI GC-MS/MS. Comparison of peak area ratios revealed a significant difference between the ischemic heart disease patients and healthy controls 2–3 h post-myocardial injury implying the possibility of NO<sub>2</sub>-OA and other nitro fatty acids to serve as indicators of myocardial injury. This observation is speculative, necessitating future investigations to confirm their potential significance as early biomarkers within a broader metabolic framework.

To our knowledge, this is the first study to perform the alkylation derivatization reaction in an untargeted metabolomics study on AMI patients and healthy controls. Remarkably, different metabolites were detected through alkylation and silylation, showing that those reactions were complementary for investigating the plasma metabolome. Through silylation, VIP features were fumaric acid, serine methyl ester, thioglycerol, acetylglycine, and D-pipecolic acid, while through alkylation, the VIP features were 3,4-dihydroxybutyric acid, malonic acid, oleic acid, homocysteine, 3-hexenedioic acid, L-beta-aspartyl-L-aspartic acid, carnosine, and 2-octenedioic acid. These features were annotated using their EI mass spectral similarity (HMDB), retention index, GC column type used, and derivatization technique.

## ASSOCIATED CONTENT

### Supporting Information

The Supporting Information is available free of charge at <https://pubs.acs.org/doi/10.1021/acs.analchem.5c05647>.

Additional experimental results for 17-Br-HDA, untargeted study QC samples and VIPs comparison spectra (PDF)

## AUTHOR INFORMATION

### Corresponding Author

Magy Herz – Department of Pharmaceutical Chemistry,  
Faculty of Pharmacy and Biotechnology, German University

in Cairo, Cairo 11835, Egypt;  orcid.org/0000-0003-0228-6877; Email: magy.maged@guc.edu.eg

## Authors

**Yasmin Elshoura** — Department of Pharmaceutical Chemistry, Faculty of Pharmacy and Biotechnology, German University in Cairo, Cairo 11835, Egypt

**Mohamed Z. Gad** — Department of Biochemistry, Faculty of Pharmacy and Biotechnology, German University in Cairo, Cairo 11835, Egypt

**Rasha Hanafi** — Department of Pharmaceutical Chemistry, Faculty of Pharmacy and Biotechnology, German University in Cairo, Cairo 11835, Egypt

Complete contact information is available at:  
<https://pubs.acs.org/10.1021/acs.analchem.5c05647>

## Notes

The authors declare no competing financial interest.

## ABBREVIATIONS

% RSD, Percentage of relative standard deviation; 17-BrHDA, 17-bromoheptadecanoic acid; ACN, Acetonitrile; AMI, Acute myocardial infarction; ATP, Adenosine triphosphate; BHT, Butylated hydroxy toluene; CAD, Coronary artery disease; CID, Collision-induced dissociation; CV, Cross-validation; CVD, Cardiovascular disease; DEE, Diethyl ether; DIPEA, N,N-diisopropylethylamine; EI, Electron impact; ESI, Electrospray ionization; FDR, False Discovery Rate; GC-MS/MS, Gas chromatography tandem mass spectrometry; H<sub>2</sub>O<sub>2</sub>, Hydrogen peroxide; HDA, Heptadecanoic acid; HMDB, Human metabolome database; HPLC, High-pressure liquid chromatography; I/R, ischemia-reperfusion; IHD, Ischemic heart disease; IPC, ischemic preconditioning; IQR, Interquartile range; IS, Internal standard; LC-MS/MS, Liquid chromatography tandem mass spectrometry; LLE, Liquid–liquid extraction; LOD, Limit of detection; LOESS, locally estimated scatterplot smoothing; LOQ, Limit of quantification; LTPRI, Linear temperature-programmed retention index; MeOH, Methanol; mRNA, messenger ribonucleic acid; MS, Mass spectrometry; MSI, Metabolomics standards initiative; MSTFA, N-methyl-N-(trimethylsilyl)trifluoroacetamide; NO<sub>2</sub>-FAs, Nitro fatty acids; NO<sub>2</sub>-LA, Nitro linoleic acid; NO<sub>2</sub>-OA, Nitro oleic acid; ONOO<sup>-</sup>, Peroxynitrite; PCA, Principal component analysis; PFB, Pentafluorobenzyl; PFB-Br, Pentafluorobenzyl bromide; PLS-DA, Partial least-squares discriminant analysis; PRESS, Predicted residual sum of squares; QC, Quality control; QSAR, Quantitative structure–activity relationship; RI, Retention index; RNS, Reactive nitrogen species; RNS, Reactive nitrogen species; ROS, Reactive oxygen species; ROS, Reactive oxygen species; Rt, Retention time; S/N, Signal-to-noise ratio; SD, Standard deviation; SEM, Standard error of the means; SPE, Solid-phase extraction; T2DM, Type 2 diabetes mellitus; TMCS, Trimethylchlorosilane; TMS, Trimethylsilyl; UPLC-ESI-MS, Ultraperformance liquid chromatography electrospray ionization-mass spectrometry; VIP, Variables influencing projection/Variable importance in projection

## REFERENCES

- (1) Kordalewska, M.; Markuszewski, M. J. Metabolomics in cardiovascular diseases. *J. Pharm. Biomed. Anal.* **2015**, *113*, 121–136.

(2) Mudaliar, M.; Thomas, F. C.; Eckersall, P. D. *Periparturient Diseases of Dairy Cows: a Systems Biology Approach*; Springer, 2017; pp. 139–183. DOI: .

(3) Guijas, C.; Montenegro-Burke, J. R.; Warth, B.; Spilker, M. E.; Siuzdak, G. Metabolomics activity screening for identifying metabolites that modulate phenotype. *Nat. Biotechnol.* **2018**, *36*, 316–320.

(4) Nalbantoglu, S.; Karadag, A.; Nalbantoglu, S.; Karadag, A. *Introductory Chapter: Insight into the OMICS Technologies and Molecular Medicine* Intech Open 2019

(5) Kiseleva, O.; Kurbatov, I.; Ilgisonis, E.; Poverennaya, E. Defining blood plasma and serum metabolome by gc-ms. *Metabolites* **2022**, *12*, 15.

(6) Melo, T.; Montero-Bullón, J. F.; Domingues, P.; Domingues, M. R. Discovery of bioactive nitrated lipids and nitro-lipid-protein adducts using mass spectrometry-based approaches. *Redox Biol.* **2019**, *23*, 101106.

(7) Mollenhauer, M.; Mehrkens, D.; Rudolph, V. Nitrated fatty acids in cardiovascular diseases. *Nitric Oxide* **2018**, *78*, 146–153.

(8) Piesche, M.; Roos, J.; Kühn, B.; Fettel, J.; Hellmuth, N.; Brat, C.; Maucher, I. V.; Awad, O.; Matrone, C.; Comerma Steffensen, S. G.; et al. The Emerging Therapeutic Potential of Nitro Fatty Acids and Other Michael Acceptor-Containing Drugs for the Treatment of Inflammation and Cancer. *Front. Pharmacol.* **2020**, *11*, 1297.

(9) Jain, K.; Siddam, A.; Marathi, A.; Roy, U.; Falck, J. R.; Balazy, M. The mechanism of oleic acid nitration by •NO<sub>2</sub>. *Free Radic Biol. Med.* **2008**, *45*, 269–283.

(10) Fazzari, M.; Trostchansky, A.; Schopfer, F. J.; Salvatore, S. R.; Sanchez-Calvo, B.; Vitturi, D.; Valderrama, R.; Barroso, J. B.; Radi, R.; Freeman, B. A.; Rubbo, H. Olives and olive oil are sources of electrophilic fatty acid nitroalkenes. *PLoS One* **2014**, *9* (1), No. e84884.

(11) Baker, P. R. S.; Schopfer, F. J.; Sweeney, S.; Freeman, B. A. Red cell membrane and plasma linoleic acid nitration products: Synthesis, clinical identification, and quantitation. *Proc. Natl. Acad. Sci. U. S. A.* **2004**, *101*, 11577–11582.

(12) Dennis, M. K.; et al. Fatty acid transduction of nitric oxide signaling: multiple nitrated unsaturated fatty acid derivatives exist in human blood and urine and serve as endogenous peroxisome proliferator-activated receptor ligands. *J. Biol. Chem.* **2005**, *280*, 42464–42475.

(13) Lima, E. S.; Di Mascio, P.; Abdalla, D. S. Cholestrylnitrolinoleate, a nitrated lipid present in human blood plasma and lipoproteins. *J. Lipid Res.* **2003**, *44* (9), 1660–1666.

(14) Rudolph, V.; Schopfer, F. J.; Khoo, N. K.; Rudolph, T. K.; Cole, M. P.; Woodcock, S. R.; Bonacci, G.; Groeger, A. L.; Golin-Bisello, F.; Chen, C. S.; et al. Nitro-fatty acid metabolome: saturation, desaturation, β-oxidation, and protein adduction. *J. Biol. Chem.* **2009**, *284* (3), 1461–1473.

(15) Tsikas, D.; Zoerner, A.; Mischke, A.; Homsi, Y.; Gutzki, F. M.; Jordan, J. Specific GC-MS/MS stable-isotope dilution methodology for free 9-and 10-nitro-oleic acid in human plasma challenges previous LC-MS/MS reports. *J. Chromatogr. B* **2009**, *877* (26), 2895–2908.

(16) Elshoura, Y.; Herz, M.; Gad, M. Z.; Hanafi, R. Nitro fatty acids: A comprehensive review on analytical methods and levels in health and disease. *Anal. Biochem.* **2024**, *694*, 115624.

(17) Herz, M. M.; Gad, M. Z.; Hanafi, R. S. Development and validation of a bioanalytical method for the quantification of nitrated fatty acids in plasma using LC-MS/MS: application to cardiovascular patients. *Separations* **2023**, *10* (2), 87.

(18) Dunn, W. B.; Broadhurst, D.; Begley, P.; Zelena, E.; Francis-McIntyre, S.; Anderson, N.; Brown, M.; Knowles, J. D.; Halsall, A.; Haselden, J. N.; et al. Procedures for large-scale metabolic profiling of serum and plasma using gas chromatography and liquid chromatography coupled to mass spectrometry. *Nat. Protoc.* **2011**, *6* (7), 1060–1083.

(19) Curvers, J. M.; Rijks, J.; Cramers, C. A.; Knauss, K.; Larson, P. Temperature programmed retention indices: Calculation from isothermal data. Part 1: Theory. *J. High Resol. Chromatogr.* **1985**, *8* (9), 607–610.

- (20) Lima, É. S.; Di Mascio, P.; Rubbo, H.; Abdalla, D. S. Characterization of linoleic acid nitration in human blood plasma by mass spectrometry. *Biochemistry* **2002**, *41* (34), 10717–10722.
- (21) Lee, L. C.; Liong, C. Y.; Jemain, A. A. Partial least squares-discriminant analysis (PLS-DA) for classification of high-dimensional (HD) data: a review of contemporary practice strategies and knowledge gaps. *Analyst* **2018**, *143* (15), 3526–3539.
- (22) Cambiaghi, A.; Ferrario, M.; Masseroli, M. Analysis of metabolomic data: tools, current strategies and future challenges for omics data integration. *Brief Bioinform.* **2016**, *18* (3), 498–510.
- (23) Tsikas, D. Measurement of nitro-oleic acid and nitro-linoleic acid in plasma by GC-MS/MS and LC-MS/MS in health and disease: The significance of the internal standard. *J. Chromatogr. B: Anal.* **2023**, *1221*, 123684.
- (24) Singh, N.; Chattree, A. *Virtual Screening of 5-(3 Chloro-1-benzothien-2 yl)-4-phenyl-4H—1, 2, 4 triazole-3-thiol derivatives And Their Potential Application On Aspergillus fumigatus*, <https://www.researchgate.net/publication/306358335>.
- (25) Tsikas, D.; Zoerner, A. A.; Mitschke, A.; Gutzki, F. M. Nitro-fatty acids occur in human plasma in the picomolar range: a targeted nitro-lipidomics GC-MS/MS study. *Lipids* **2009**, *44* (9), 855–865.
- (26) Tsikas, D.; Zoerner, A. A.; Jordan, J. Oxidized and nitrated oleic acid in biological systems: Analysis by GC-MS/MS and LC-MS/MS, and biological significance. *Biochim. Biophys. Acta Mol. Cell Biol. Lipids* **2011**, *1811* (11), 694–705.
- (27) Trettin, A.; Böhmer, A.; Zoerner, A. A.; Gutzki, F. M.; Jordan, J.; Tsikas, D. GC-MS/MS and LC-MS/MS studies on unlabelled and deuterium-labelled oleic acid (C18: 1) reactions with peroxynitrite (ONOO<sup>-</sup>) in buffer and hemolysate support the pM/nM-range of nitro-oleic acids in human plasma. *J. Chromatogr. B* **2014**, *964*, 172–179.
- (28) Stokvis, E.; Rosing, H.; Beijnen, J. H. Stable isotopically labeled internal standards in quantitative bioanalysis using liquid chromatography/mass spectrometry: necessity or not? *Rapid Commun. Mass Spectrom.* **2005**, *19* (3), 401–407.
- (29) Chemical book. *17-BROMOHEPTADECANOIC ACID*. <https://www.chemicalbook.com/msds/17-bromoheptadecanoic-acid.htm>.
- (30) Moldoveanu, S. C.; David, V. Derivatization methods in GC and GC/MS. In *Gas Chromatography-Derivatization, Sample Preparation Application*; IntechOpen, 2018. DOI: .
- (31) Tsikas, D. Pentfluorobenzyl bromide—A versatile derivatization agent in chromatography and mass spectrometry: I. Analysis of inorganic anions and organophosphates. *J. Chromatogr. B* **2017**, *1043*, 187–201.
- (32) Zwiener, C.; Frimmel, F. H. LC-MS analysis in the aquatic environment and in water treatment? A critical review. *Anal. Bioanal. Chem.* **2004**, *378* (4), 851–861.
- (33) Nadtochiy, S. M.; Baker, P. R.; Freeman, B. A.; Brookes, P. S. Mitochondrial nitroalkene formation and mild uncoupling in ischaemic preconditioning: implications for cardioprotection. *Cardiovasc. Res.* **2009**, *82* (2), 333–340.
- (34) Rudolph, V.; Rudolph, T. K.; Schopfer, F. J.; Bonacci, G.; Woodcock, S. R.; Cole, M. P.; Baker, P. R.; Ramani, R.; Freeman, B. A. Endogenous generation and protective effects of nitro-fatty acids in a murine model of focal cardiac ischaemia and reperfusion. *Cardiovasc. Res.* **2010**, *85* (1), 155–166.
- (35) Schopfer, F. J.; Cipollina, C.; Freeman, B. A. Formation and signaling actions of electrophilic lipids. *Chem. Rev.* **2011**, *111* (10), 5997–6021.
- (36) Padilla, M. N.; Mata-Pérez, C.; Melguizo, M.; Barroso, J. B. In vitro nitro-fatty acid release from Cys-NO<sub>2</sub>-fatty acid adducts under nitro-oxidative conditions. *Nitric Oxide* **2017**, *68*, 14–22.
- (37) Chirikan, A.; Ezzaky, S.; Eloual, I.; Madani, A.; Jroundi, L.; Laamrani, F. Z. Jejunal intussusception on jejunostomy tube: a rare cause of occlusion in adults. *J. Surg. Case Rep.* **2022**, *97*, 107447.
- (38) Alonso, A.; Marsal, S.; Julià, A. Analytical methods in untargeted metabolomics: state of the art in 2015. *Front. Bioeng. Biotechnol.* **2015**, *3*, 23.
- (39) Ali, S. E.; Farag, M. A.; Holvoet, P.; Hanafi, R. S.; Gad, M. Z. A comparative metabolomics approach reveals early biomarkers for metabolic response to acute myocardial infarction. *Sci. Rep.* **2016**, *6* (1), 36359.
- (40) Zhang, Q.; Wang, G.; A, J.; Ma, B.; Dua, Y.; Zhu, L.; Wu, D. Metabonomic profiling of diet-induced hyperlipidaemia in a rat model. *Biomarkers* **2010**, *15* (3), 205–216.
- (41) Szymańska, E.; Saccenti, E.; Smilde, A. K.; Westerhuis, J. A. Double-check: validation of diagnostic statistics for PLS-DA models in metabolomics studies. *Metabolomics* **2012**, *8* (Suppl 1), 3–16.
- (42) Westerhuis, J. A.; Hoefsloot, H. C.; Smit, S.; Vis, D. J.; Smilde, A. K.; van Velzen, E. J.; van Duijnhoven, J. P.; van Dorsten, F. A. Assessment of PLSDA cross validation. *Metabolomics* **2008**, *4* (1), 81–89.
- (43) Lindgren, F.; Hansen, B.; Karcher, W.; Sjöström, M.; Eriksson, L. Model validation by permutation tests: applications to variable selection. *J. Chemom.* **1996**, *10* (5–6), 521–532.
- (44) Pesarin, F.; Salmaso, L. *Permutation tests for complex data: theory, applications and software*; John Wiley & Sons, 2010.
- (45) Westerhuis, J. A.; van Velzen, E. J.; Hoefsloot, H. C.; Smilde, A. K. Discriminant Q<sub>2</sub> (DQ2) for improved discrimination in PLSDA models. *Metabolomics* **2008**, *4* (4), 293–296.
- (46) Zhou, J.; Hou, H. T.; Song, Y.; Zhou, X. L.; Chen, H. X.; Zhang, L. L.; Xue, H. M.; Yang, Q.; He, G. W. Metabolomics analysis identifies differential metabolites as biomarkers for acute myocardial infarction. *Biomolecules* **2024**, *14* (5), 532.
- (47) Zimmerman, J.; Fromm, R.; Meyer, D.; Boudreault, A.; Wun, C. C.; Smalling, R.; Davis, B.; Habib, G.; Roberts, R. Diagnostic marker cooperative study for the diagnosis of myocardial infarction. *Circulation* **1999**, *99* (13), 1671–1677.
- (48) Rizza, R. A.; Mandarino, L. J.; Gerich, J. E. Cortisol-induced insulin resistance in man: impaired suppression of glucose production and stimulation of glucose utilization due to a postreceptor defect of insulin action. *J. Clin. Endocrinol. Metab.* **1982**, *54* (1), 131–138.
- (49) Gogna, N.; Krishna, M.; Oommen, A. M.; Dorai, K. Investigating correlations in the altered metabolic profiles of obese and diabetic subjects in a South Indian Asian population using an NMR-based metabolomic approach. *Mol. Biosyst.* **2014**, *11* (2), 595–606.
- (50) Christensen, N. J.; Videbaek, J. Plasma catecholamines and carbohydrate metabolism in patients with acute myocardial infarction. *J. Clin. Invest.* **1974**, *54* (2), 278–286.
- (51) Teul, J.; Rupérez, F. J.; Garcia, A.; Vaysse, J.; Balyssac, S.; Gilard, V.; Malet-Martino, M.; Martin-Ventura, J. L.; Blanco-Colio, L. M.; Tuñón, J.; et al. Improving metabolite knowledge in stable atherosclerosis patients by association and correlation of GC-MS and 1H NMR fingerprints. *J. Proteome Res.* **2009**, *8* (12), 5580–5589.
- (52) Stamler, J. S.; Osborne, J. A.; Jaraki, O.; Rabbani, L. E.; Mullins, M.; Singel, D.; Loscalzo, J. Adverse vascular effects of homocysteine are modulated by endothelium-derived relaxing factor and related oxides of nitrogen. *J. Clin. Invest.* **1993**, *91* (1), 308–318.
- (53) Dardik, R.; Varon, D.; Tamarin, I.; Zivelin, A.; Salomon, O.; Shenkman, B.; Savion, N. Homocysteine and oxidized low density lipoprotein enhance platelet adhesion to endothelial cells under flow conditions: distinct mechanisms of thrombogenic modulation. *Thromb. Haemost.* **2000**, *83* (2), 338–344.
- (54) Ganguly, P.; Alam, S. F. Role of homocysteine in the development of cardiovascular disease. *Nutr. J.* **2015**, *14* (1), 6.
- (55) Tsai, J.C.; Perrella, M.A.; Yoshizumi, M.; Hsieh, C.M.; Haber, E.; Schlegel, R.; Lee, M.E. Promotion of vascular smooth muscle cell growth by homocysteine: a link to atherosclerosis. *Proc. Natl. Acad. Sci. U. S. A.* **1994**, *91*, 6369–6373.
- (56) de Courten, B.; Kurdiava, T.; de Courten, M. P.; Belan, V.; Everaert, I.; Vician, M.; Teede, H.; Gasperikova, D.; Aldini, G.; Derave, W.; et al. Muscle carnosine is associated with cardiometabolic risk factors in humans. *PLoS One* **2015**, *10* (10), No. e0138707.
- (57) PubChem *L-beta-aspartyl-L-aspartic acid*, PubChem: <https://pubchem.ncbi.nlm.nih.gov/compound/L-beta-aspartyl-L-aspartic-acid>.

- (58) Curovic, V.R.; Sørland, B.A.; Hansen, T.W.; Jain, S.Y.; Sulek, K.; Mattila, I.M.; Frimodt-Møller, M.; Trost, K.; Legido-Quigley, C.; Theilade, S.; et al. Circulating metabolomic markers in association with overall burden of microvascular complications in type 1 diabetes. *BMJ Open Diab. Res. Care* **2024**, *12* (2), No. e003973.
- (59) Matalon, R.; Michaels, K.; Kaul, R.; Whitman, V.; Rodriguez-Novo, J.; Goodman, S.; Thorburn, D. Malonic aciduria and cardiomyopathy. *J. Inherit. Metab. Dis.* **1993**, *16* (3), 571–573.
- (60) Surendran, A.; Atefi, N.; Zhang, H.; Aliani, M.; Ravandi, A. Defining acute coronary syndrome through metabolomics. *Metabolites* **2021**, *11* (10), 685.
- (61) Lin-Holderer, J.; Li, L.; Gruneberg, D.; Marti, H. H.; Kunze, R. Fumaric acid esters promote neuronal survival upon ischemic stress through activation of the Nrf2 but not HIF-1 signaling pathway. *Neuropharmacology* **2016**, *105*, 228–240.
- (62) Wu, C.; Chen, H. C.; Chen, S. T.; Chiang, S. Y.; Wu, K. Y. Elevation in and persistence of multiple urinary biomarkers indicative of oxidative DNA stress and inflammation: Toxicological implications of maleic acid consumption using a rat model. *PLoS One* **2017**, *12* (10), No. e0183675.
- (63) Gundogdu, G.; Senol, O.; Demirkaya Miloglu, F.; Koza, Y.; Gundogdu, F.; Hacimüftüoğlu, A.; Abd El-Aty, A. M. Serum metabolite profiling of ST-segment elevation myocardial infarction using liquid chromatography quadrupole time-of-flight mass spectrometry. *Biomed. Chromatogr.* **2020**, *34* (2), No. e4738.
- (64) Wang, L.; Hou, E.; Wang, Z.; Sun, N.; He, L.; Chen, L.; Liang, M.; Tian, Z. Analysis of metabolites in plasma reveals distinct metabolic features between Dahl salt-sensitive rats and consomic SS. 13BN rats. *Biochem. Biophys. Res. Commun.* **2014**, *450* (1), 863–869.
- (65) Tian, Z.; Greene, A. S.; Usa, K.; Matus, I. R.; Bauwens, J.; Pietrusz, J. L.; Cowley, A. W., Jr; Liang, M. Renal regional proteomes in young Dahl salt-sensitive rats. *Hypertension* **2008**, *51* (4), 899–904.
- (66) Tian, Z.; Liu, Y.; Usa, K.; Mladinov, D.; Fang, Y.; Ding, X.; Greene, A. S.; Cowley, A. W., Jr; Liang, M. Novel role of fumarate metabolism in dahl-salt sensitive hypertension. *Hypertension* **2009**, *54* (2), 255–260.
- (67) Panchal, A. R.; Comte, B.; Huang, H.; Dudar, B.; Roth, B.; Chandler, M.; Des Rosiers, C.; Brunengraber, H.; Stanley, W. C. Acute hibernation decreases myocardial pyruvate carboxylation and citrate release. *Am. J. Physiol. Heart Circ. Physiol.* **2001**, *281* (4), H1613–20.
- (68) Zhang, S.; Gao, W.; Xie, L.; Zhang, G.; Wei, Z.; Li, J.; Song, C.; Chang, M. Malonic acid shapes bacterial community dynamics in compost to promote carbon sequestration and humic substance synthesis. *Chemosphere* **2024**, *350*, 141092.
- (69) Jaswal, J. S.; Keung, W.; Wang, W.; Ussher, J. R.; Lopaschuk, G. D. Targeting fatty acid and carbohydrate oxidation—a novel therapeutic intervention in the ischemic and failing heart. *Biochim. Biophys. Acta - Mol. Cell Res.* **2011**, *1813* (7), 1333–1350.
- (70) Jasbi, P.; Nikolich-Žugich, J.; Patterson, J.; Knox, K. S.; Jin, Y.; Weinstock, G. M.; Smith, P.; Twigg, H. L., III; Gu, H. Targeted metabolomics reveals plasma biomarkers and metabolic alterations of the aging process in healthy young and older adults. *GeroScience* **2023**, *45* (6), 3131–3146.
- (71) Tserng, K. Y.; Jin, S. J. Metabolic origin of urinary 3-hydroxydicarboxylic acids. *Biochemistry* **1991**, *30* (9), 2508–2514.
- (72) Adeva-Andany, M.; Souto-Adeva, G.; Ameneiros-Rodríguez, E.; Fernández-Fernández, C.; Donapetry-García, C.; Domínguez-Montero, A. Insulin resistance and glycine metabolism in humans. *Amino Acids* **2018**, *50* (1), 11–27.
- (73) Almanza-Perez, J. C.; Alarcon-Aguilar, F. J.; Blancas-Flores, G.; Campos-Sepulveda, A. E.; Roman-Ramos, R.; Garcia-Macedo, R.; Cruz, M. Glycine regulates inflammatory markers modifying the energetic balance through PPAR and UCP-2. *Biomed. Pharmacother.* **2010**, *64* (8), 534–540.
- (74) Vallée, A.; Lecarpentier, Y. Crosstalk between peroxisome proliferator-activated receptor gamma and the canonical WNT/ $\beta$ -catenin pathway in chronic inflammation and oxidative stress during carcinogenesis. *Front. Immunol.* **2018**, *9*, 745.
- (75) Tibbetts, A. S.; Appling, D. R. Compartmentalization of Mammalian folate-mediated one-carbon metabolism. Annual review of nutrition. *Annu. Rev. Nutr.* **2010**, *30* (1), 57–81.
- (76) Liu, Y.; Liu, J. E.; He, H.; Qin, M.; Lei, H.; Meng, J.; Liu, C.; Chen, X.; Luo, W.; Zhong, S. Characterizing the metabolic divide: distinctive metabolites differentiating CAD-T2DM from CAD patients. *Cardiovasc. Diabetol.* **2024**, *23* (1), 14.
- (77) Ouyang, Y.; Qiu, G.; Zhao, X.; Su, B.; Feng, D.; Lv, W.; Xuan, Q.; Wang, L.; Yu, D.; Wang, Q.; et al. Metabolome-genome-wide association study (mGWAS) reveals novel metabolites associated with future type 2 diabetes risk and susceptibility loci in a case-control study in a Chinese prospective cohort. *Global Chall.* **2021**, *5* (4), 2000088.
- (78) Gu, X.; Al Dubayee, M.; Alshahrani, A.; Masood, A.; Benabdulkamel, H.; Zahra, M.; Li, L.; Abdel Rahman, A. M.; Aljada, A. Distinctive metabolomics patterns associated with insulin resistance and type 2 diabetes mellitus. *Front. Mol. Biosci.* **2020**, *7*, 609806.
- (79) Priyadarsini, S.; McKay, T.B.; Sarker-Nag, A.; Allegood, J.; Chalfant, C.; Ma, J.X.; Karamichos, D. Complete metabolome and lipidome analysis reveals novel biomarkers in the human diabetic corneal stroma. *Exp. Eye Res.* **2016**, *153*, 90–100.
- (80) Griffin, J. L.; Atherton, H.; Shockcor, J.; Atzori, L. Metabolomics as a tool for cardiac research. *Nat. Rev. Cardiol.* **2011**, *8* (11), 630–643.



CAS BIOFINDER DISCOVERY PLATFORM™

## CAS BIOFINDER HELPS YOU FIND YOUR NEXT BREAKTHROUGH FASTER

Navigate pathways, targets, and diseases with precision

**Explore CAS BioFinder**